

**The initial phases of the 2008-2009 Mt. Etna eruption:  
a multi-disciplinary approach for hazard assessment**

Bonaccorso A., Bonforte A., Calvari S., Del Negro C., Di Grazia G., Ganci G., Neri M., Vicari A., Boschi E.

Istituto Nazionale di Geofisica e Vulcanologia

Sezione di Catania

**Submitted to the Journal of Geophysical Research,**

Submitted, August, 2010

Revised, 22 December 2010

(minor revisions)

Contact details :

Alessandro Bonaccorso

Istituto Nazionale di Geofisica e Vulcanologia

Sezione di Catania

Piazza Roma, 2

95123 Catania, Italy

Ph. +39.095.7165800

Fax. +39.095.435801

Email : [bonaccorso@ct.ingv.it](mailto:bonaccorso@ct.ingv.it)

Running head :

Etna 2008 eruption multi-disciplinary hazard assessment

## **Abstract**

Between 2007 and early 2008, the INGV monitoring networks on Etna volcano recorded a recharging phase that climaxed with a new effusive eruption on 13 May 2008, and lasted about 14 months. A dike-forming intrusion was accompanied by a violent seismic swarm, with more than 230 events recorded in the first six hours, the largest being  $M_L = 3.9$ . In the meanwhile, marked ground deformation was recorded by the permanent tilt and GPS networks, and sudden changes in the summit area were detected by five continuously recording magnetic stations. Poor weather conditions did not allow direct observation of the eruptive events, but important information was provided by infrared satellite images that detected the start of lava fountains from the eruptive fissure, feeding a lava flow. This flow spread within the Valle del Bove depression, covering 6.4 km on the south-eastern flank of the volcano in a few hours. The seismicity and deformation pattern indicated that the dike-forming intrusion was propagating northwards. It produced a dry fracture field, which generated concern for the possibility that the eruptive fissures could expand downslope towards populated areas. Monitoring and modeling of the multi-disciplinary data, together with the simulations of ash dispersal and lava flows, allowed us both to infer the eruptive mechanisms and provide a correct interpretation of the ongoing phenomena, furnishing useful information for civil defense purposes. We describe how this approach of feedback between monitoring and research provides critical support to risk evaluation.

## **1. Introduction**

In the last few decades, several eruptions have taken place on Mt. Etna in relatively short succession (approximately one event every two years) [e.g. *Branca and Del Carlo, 2004; Allard et al., 2006*], with lava flows causing serious damage to agriculture and crops, destroying roads and railway lines and dangerously threatening - fortunately without invading them - a number of towns. There have been numerous interventions urged by the Italian government to boost the monitoring systems and mitigate volcanic hazards, such as attempts to divert lava flows that threatened urban settlements

[*Barberi et al.*, 1993; *Barberi et al.*, 2003]. After the start of the new millennium, the most recent eruptions have also been characterized by prolonged explosive activity and ash emission that have created varying degrees of adversity to the Etnean cities and towns, and have often posed major problems – even paralyzing – to air traffic to and from the international airport of Catania. For this volcano particularly, the problem of understanding eruptive phenomena is of notable importance and also of considerable impact, owing to the high population density (about 1,200,000 people) on its slopes.

In recent years, the observations and monitoring systems on Etna have been significantly upgraded by the Istituto Nazionale di Geofisica e Vulcanologia (INGV), the scientific institution assigned to monitor and survey active Italian volcanoes. The quantity and quality of instrumental data, associated with the frequent recent eruptions, have enabled a better understanding of the phenomena in progress and also to model different eruptive mechanisms. In particular, the INGV monitors and studies Etna volcano through its Department in Catania (INGV-CT) by a multi-disciplinary surveillance [for a review of the activities and studies see *Bonaccorso et al.*, 2004a]. The INGV-CT maintains different monitoring networks formed by hundreds of permanent stations (seismic, GPS, tilt, visual and thermal webcams, gravity, magnetic, geochemical, etc.), manages the H24 surveillance service for the Civil Defense Department of the Italian government and gives prompt alert and updates on volcanic activity occurring in southern Italy.

Following a sequence of rather dramatic and destructive eruptions between 2001 and 2006, Etna started a new recharging phase from 2007. This culminated with a dike-forming intrusion on 13 May 2008 and was accompanied by a strong seismic release, marked permanent ground deformation, sudden magnetic changes and by violent lava fountaining characterizing the first phase of the eruption.

The exceptional instrumental quantity and quality of data, coupled with the frequent recent Etna eruptions, have enabled modelling different eruptive mechanisms, leading to a better understanding of the phenomena in progress. The work presented here, besides focusing on the last eruption begun in May 2008 and lasted about one year, comprises important innovative aspects concerning the knowledge

of eruptive mechanisms from a broad and multi-disciplinary perspective, and simulations of ongoing volcanic processes such as ash dispersal and lava flow expansion.

After an overview on the recent eruptive activity of Etna (Section 2), in Section 3 we describe the recharging phase which preceded the eruption. Then the crucial moments of the beginning of the eruption with the first important stages of the dike-forming intrusion are outlined. We describe the intrusion and eruption characteristics in Section 4, highlighting the peculiarity of this event on the basis of seismicity, seismic tremor analysis, ground deformation, and geophysical signals, accompanied by an analysis of the extensive ground fracture field formed on the highest northern sector of Etna. In Section 5, the modeling results on the 2008 dike intrusion are also presented. In Section 6, the main hazard implications of this eruption are discussed, describing the lava flows and ash plume simulations applied to face this eruption that proved extremely useful for civil protection purposes. Finally, in Section 7 we discuss the interpretation of this eruption, the explanation of its new emplacement mechanisms, the general implications for volcano hazard and how we managed them.

## **2. Recent eruptive activity at Mt. Etna**

Mt. Etna volcano is located in southern Italy (Sicily) and is the highest active volcano in Europe recently measured at 3329 m [*Neri et al.*, 2008]. During the past 400 years, the volcano has produced over sixty flank eruptions [*Behncke and Neri*, 2003a; *Branca and Del Carlo*, 2004; *Behncke et al.*, 2005], while the summit craters have been almost continuously active, with persistent degassing and frequent explosive activity at the vents on the crater floor (Fig. 1).

The 1991-1993 flank eruption [*Calvari et al.*, 1994; *Stevens et al.*, 1997] was the most important eruption in the last three centuries both in terms of duration (472 days) and volume of lava erupted (about  $235 \times 10^6 \text{ m}^3$ ). Immediately following the eruption, the volcano showed a persistent degassing (April 1993–June 1995), then an almost continuous summit activity, increasing in intensity between July 1995 and June 2001 [*Allard et al.*, 2006]. Between 1993 and 2001, an overall recharging phase is

well documented by the (is clearly observable in the) ground deformation, which showed an almost continuous expansion of the whole volcano edifice [e.g. *Bonaccorso and Davis, 2004; Bonaccorso et al., 2006; Bonforte et al., 2008*]. This phase culminated with the two violent and dramatic explosive-effusive flank eruptions of July-August 2001 and October 2002 – January 2003 [*Behncke and Neri, 2003b; Andronico et al., 2005*]. Dike-forming intrusions related to both eruptions followed an eccentric path (i.e. bypassed the central conduit system; *Acocella and Neri, 2003*) on the S flank, resulting in strong and prolonged explosive activity, intense seismicity, and marked ground deformation. Conversely, the NE branches of the 2001 and 2002-2003 eruptive fissures oriented directly from the central conduit, producing an eruption with a different composition of largely degassed magma [*Behncke and Neri, 2003b; Andronico et al., 2005*]. The unusual and long-lasting explosive activity from the S fissures caused major problems for road traffic and disrupted air travel at the International Airport of Catania. Lava flows in 2001 expanded south and threatened the village of Nicolosi (Fig. 1). The NE lateral intrusion in 2002-2003 also promoted a marked acceleration of the eastward sliding of the SE flank of the volcano, therefore marking a significant change in the volcano's dynamic regime [e.g. *Neri et al., 2004, 2005, 2009; Rust et al., 2005; Walter et al., 2005; Bonaccorso et al., 2006; Bonforte et al., 2007, 2009; Puglisi et al., 2008; Ruch et al., 2010*].

After these flank eruptions and between 2003 and 2008, the volcano showed two interesting phenomena: *i*) a renewal of moderate inflation/deflation cycles both preceding and accompanying the 2004-2005 and 2006 flank eruptions, and *ii*) a constant and marked eastward sliding of the eastern flank of the volcano [*Bonforte et al., 2008; Neri et al., 2009; Solaro et al., 2010*]. The effusive activity in 2004-2005 was fed by a dike-like intrusion that intersected the central conduit of the volcano [*Burton et al., 2005; Neri and Acocella, 2006*]. This eruption was relatively 'passively' triggered, in the sense that the draining fissures were caused by the exceptional sliding rate (~ 7-10 cm/y) recorded in the eastern flank of the volcano by the GPS network [*Bonaccorso et al., 2006*]. As a result, the eruption onset was unusually 'silent', because it was neither a forerunner nor accompanied by the common explosive activity at the summit craters. There was no significant increase in the gas emission from the summit craters, no seismic swarms, seismic tremor or seismicity of any kind, no ground deformation changes,

all phenomena that are usually observed during an intrusion process on Mt Etna [Burton *et al.*, 2005; Bonaccorso *et al.*, 2006].

After the end of the 2004-2005 eruption, the GPS network recorded a renewal of the type of inflation precursor that led to the 2006 eruptions. Besides the inflation-deflation sequence preceding and following lava output (Fig. 2), the eastern flank of the volcano showed seemingly independent dynamics with a fairly constant seaward motion [Puglisi and Bonforte, 2004; Bonforte and Puglisi, 2006; Bonaccorso *et al.*, 2006; Neri *et al.*, 2009; Solaro *et al.*, 2010]. The 2006 eruptions marked the reactivation of the South-East Crater (SEC), figure 1, that had been inactive since July 2001 [Neri *et al.*, 2006]. Strombolian activity and lava overflows characterized the summit vent of this crater, and were accompanied by lava emission from WNW-ESE fissures that opened at the base of the cone [Behncke *et al.*, 2008, 2009]. In similarity with the 2004-2005 phase, the onset of the 2006 July eruption was not accompanied by evident changes of geophysical parameters, including seismicity or significant explosive activity from the summit craters [Behncke *et al.*, 2008].

After the end of the 2006 eruptive phases, the GPS network indicated again a volcano inflation (Fig. 2d) [Aloisi *et al.*, 2009]. However this time, unlike the previous 2004-2005 and 2006 cases, the 2008-2009 eruption was preceded by clear volcanological precursors, such as the several lava fountaining episodes which occurred from March 2007 until 10 May 2008. Moreover, since January 2008, the seismic network recorded a strong increase in seismicity mainly due to many seismic swarms taking place in the southern and western flanks of the volcano (Fig. 3) [<http://www.ct.ingv.it>]. The recharge phase culminated with the 13 May 2008 – 6 July 2009 flank eruption, which we describe in this paper focusing mainly in the initial phase.

### **3. The 2007-2008 recharging phase**

#### **3.1 The activity of January 2007 – April 2008 : the preparatory phase**

After the deflation of the volcano edifice associated with the 2006 eruptions (Fig. 2c), during 2007 and until 12 May 2008 a radial centrifugal pattern of the displacement vectors was recorded by the GPS network (Fig. 2d). The areal dilatation of the volcano edifice showed a nearly constant positive trend, recovering the contraction that cumulated during the 2006 eruptions. During this period, more than 1200 earthquakes with magnitude ranging from 0.7 to 3.3 were recorded by the local permanent seismic network managed by INGV, comprising 26 seismic stations installed on the flanks of the volcano [<http://www.ct.ingv.it>]. About half of the earthquakes were relatively localized, as shown in figure 3a, b. The spatial distribution of seismicity showed a fairly usual seismic pattern for Mt. Etna: most of the events were localized in the eastern side of the volcanic area, while deeper focal depths characterize the western side. Higher rates of occurrence and shallower foci (< 5 km) were recorded in the eastern flank, while the deeper seismicity on the western side (more than 10 km below sea level) was linked to the regional structural systems trending NE-SW and NNW-SSE [Gresta *et al.*, 1990]. An acceleration in the strain release curve took place on 7 January 2008 in concomitance with a deep seismic swarm (30 events,  $M_{\max}=2.8$ ) in the SW sector of the volcanic area (Fig. 3c). Some days later, on January 12, another deep seismic swarm occurred in a neighboring area (14 events,  $M_{\max}=3.2$ ) in the W flank. Thus, the temporal distribution of seismicity preceding the 2008-2009 eruption highlights a volcano unrest period of a few months before the beginning of the volcanic activity.

During 2007-2008, the eruptive activity of Etna was characterized by seven episodes of lava fountains from SEC accompanied by lava flow emission. The first six occurred during 2007 on 29 March, 11 April, 29 April, 7 May, 4-5 September, and 23 November, with activity changing from intense strombolian explosions to lava fountaining and sustained eruption columns, accompanied by lava outflow from fissures opened at the base of the SEC cone in WNW-ESE, N-S and E-W directions. The last two episodes of 2007 were characterized by strong lava fountaining, tephra emission and the production of extensive lava flows [Andronico *et al.*, 2009]. In particular, the 4-5 September lava fountaining lasted for an unusually long time (more than 10 hours) with the same strong intensity, and produced a ~4.6 km long lava flow field into the Valle del Bove.

### 3.2 The 10 May 2008 lava fountain : the prelude

On 10 May 2008 one of the most violent explosive phases since 2003 occurred at Mt. Etna, anticipating by only three days the next effusive and long-lasting flank eruption. Starting at ~14:00 GMT a new vent opened at the eastern base of the SEC (Fig. 4). This vent erupted intense lava fountaining characterized by an unusually high rate that fed a lava field covering ~ 2 km<sup>2</sup> of land in the barren Valle del Bove in only 4-5 hours and reaching a length of 6.4 km. An approximate estimation of the erupted volume, calculated on the basis of a mean lava flow thickness of 0.5 meters, is ~0.7 10<sup>6</sup> m<sup>3</sup>.

Volcanic thermal anomalies were automatically detected by SEVIRI infrared channels (spatial resolution 3 km<sup>2</sup> at Nadir, temporal resolution 15 minutes) on board the Meteosat satellite during the 10 May lava fountain from 14:00 to 19:00 GMT. The whole time period was characterized by thick cloud cover, a condition that causes an underestimation of the radiance values. Despite this meteorological situation, this fountain was determined to be the most powerful of those recorded by SEVIRI sensor between 2007 and 2008, reaching at 15:00 GMT a maximum value of measured radiative power of ~ 15 GW. In figure 5, the behavior of cumulative radiative power calculated at all hot pixels per image is reported for the whole period of the fountain. For three significant instants - the beginning (14:00 GMT), the strongest phase (15:00 GMT) and the decreasing phase (17:30 GMT) of activity - the geospatial location of the detected anomalous pixels is shown on a Google Map Service base. The colors of the pixels are associated with the intensity of the radiative power calculated for each pixel. Starting from the radiative power, it is possible to compute an estimation of the effusion rate [*Harris et al.*, 2005; *Vicari et al.*, 2009], finding a mean value of about 25 m<sup>3</sup>s<sup>-1</sup>. However, given the filtering effect provided by clouds covering the eruptive zone, the radiative power, and thus the effusion rate may be underestimated. Nonetheless, using the formula proposed by *Calvari and Pinkerton* [1998], a mean effusion rate of 30 m<sup>3</sup> s<sup>-1</sup> is needed in order to obtain a 6.4 km long lava flow. The ash plume dispersed first towards N, then rotated NE with an ash fallout affecting a wide area on the N and NE lower flanks of the volcano. At 17:00 GMT, the ash plume dispersal also impacted the airport of Reggio Calabria (distant ~ 100 km from Catania), increasing concerns for the possible disruption of air traffic. However, by that time the explosive and effusive activity had gradually decreased, and by 18:00 GMT



on the same day a decrease of volcanic tremor accompanied the end of the explosive and effusive activities. No eruptive activity characterized the summit of Mt. Etna for three days, when eventually a new explosive and effusive phase resumed fairly close to the northern base of the SEC.

#### **4. The 2008-2009 flank eruption**

On 13 May 2008 a strong shallow seismic swarm preceded and accompanied the onset of the eruption (Fig. 3). Between 08:39 and 15:52 GMT, in the north-eastern summit area of the volcano, 241 earthquakes were recorded, most of them occurring in the first two hours. The depths of the foci ranged between 1.5 km below sea level (bsl) and 1.5 km above sea level (asl), tending to be shallower towards the N. The most energetic events were recorded at 10:07 ( $M_D=3.2$ ) and 12:13 GMT ( $M_D=3.3$ ). The spatio-temporal distribution of the earthquakes clearly showed an attempt of the feeder dike-forming intrusion to migrate in the northern sector of the summit area of the volcano from the beginning of the swarm until 09:30 GMT (Fig. 6). From 09:30 GMT onwards, coincident with the beginning of the lava fountaining from the eruptive fissure, the number of earthquakes drastically decreased and the rupture locations turned back toward S in the area where the eruptive fissure eventually opened.

A description of the uprising magma intrusion was provided by the tremor source location performed by using a grid-search approach [*Gottschammer and Surono, 2000; Battaglia et al., 2005; Di Grazia et al., 2006, 2009*]. A few hours before the beginning of the eruption, volcanic tremor showed significant variation both in the amplitude and the source location (Fig. 7). Starting from 06:40 GMT, the tremor source locations tended to be shallower and moving towards the E (Fig 7a, b). Such a sharp migration of the tremor source centroid highlighted the imminence of the eruption as well as the magma pathway and the eruptive fissure position. The volcanic tremor amplitude rapidly increased at the same time as the source migration and reached its maximum at 10:10 GMT, exceeding the maximum level recorded during the lava fountain on 10 May 2008 (Fig. 7c). Afterwards, the tremor amplitude abruptly

decreased in the successive hours and then more slowly decreased on the following days [Patanè, 2008].

Due to the cloud cover and fog around the volcano, the permanent webcams network was not able to record the explosive activity. However, important information was provided by the SEVIRI sensor. In figure 8 the SEVIRI sequence is recorded from 9:15 to 10:30 GMT, when it was possible to track the evolution of the ash plume (yellow pixels) until the first hot spot related to eruptive activity (red pixels). No eruptive phenomena are observable in the image acquired at 9:15 GMT. The next image acquired at 9:30 GMT detected the beginning of an ash plume moving towards the NE, which was associated with the lava fountain from the northern part of the eruptive fissure. Instead, the first hot spot, due to the increased lava output and thermal anomaly, was detected at 10:30 GMT.

Coincident with the beginning of the lava fountaining and lava flow output from the eruptive fissure, images from Moderate Resolution Imaging Spectrometer (MODIS) aboard EOS satellites (spatial resolution 1 km<sup>2</sup>, temporal resolution 6 hours) were also analyzed showing the first hot spot at 9:45 GMT. This coarse resolution is owing to the fact that the ground-projected area of SEVIRI's IFOV (instant field of view) is more than one order of magnitude greater than that of MODIS, thus it cannot distinguish thermal anomalies as small as those detectable by the MODIS [Roberts *et al.*, 2005]. Radiative transfer modeling suggests that SEVIRI should be able to detect and characterize volcanic events whose radiative power ranges from 100 to 1000 MW per pixel, implying that for the typical range of volcanic eruption temperatures (900-1200° K), the minimum area detectable should be of about 100 m<sup>2</sup> [Roberts *et al.*, 2005].

The eruption initiated with a system of eruptive fissures propagating SE from the summit craters toward the western wall of the Valle del Bove. Lava fountains erupted from a N140°E fissure extending between 3050 and 2950 m asl. In two hours, the eruptive fissure propagated downslope and southeastward, curving N120°E, and reaching the minimum elevation of 2620 m asl (Fig. 9). Meanwhile, strombolian activity migrated from the upper segment of the fissure to its lowest portion. Here, a lava flow erupted at high rates from two main vents (V1 and V2 in figure 9) and rapidly expanded in the barren Valle del Bove, reaching 6 km in length and the lowest elevation of 1300 m asl.

After the initial phase of the eruption, when the lavas emerged from a N140-120°E fissure (3050-2620 m asl), a ~N-S dry, 2450 m long and 200-800 m wide asymmetric graben, formed in the upper portion of the NE Rift (3320-2620 m asl), in a roughly flat area (i.e. dipping ~5-10° N). Fractures in this area were high-angle extensional features across which the ground surface was horizontally displaced by up to 0.1 m, with a maximum vertical movement of 0.2 m. This fracture field grew for a few hours, presumably until the early afternoon on 13 May, because poor weather conditions did not allow continuous observations. The extension and the geometry of the graben were compatible with a northward dike-forming intrusion located at a depth of about 800 m with respect to the topographic surface [Pollard *et al.*, 1983; McGuire *et al.*, 1991; Day *et al.*, 1999; Billi *et al.*, 2003]. No eruptive activity was involved with these fractures.

The lava flow emplaced on 13 May expanded within the upper Valle del Bove and reached a maximum distance of 6.4 km on the first day. The following days the effusion rate showed a marked decline (Fig. 10), accompanied by a gradual up-slope migration of the active lava flow fronts, by deepening of the lava level within the master channel, and by a decrease in the intensity of the explosive activity from the uppermost portion of the eruptive fissure. The decline in magma supply and the drainage of the feeder dike resulted, by the end of May, in an obstruction and inward collapse of the walls of the SEC summit crater and of the effusive vent zone at its eastern base, choking off the magma supply allowing to build up within the volcano causing a further up-slope migration of the active flow fronts, from 1300 m to 2200 m asl. After this date, a sudden increase in seismic tremor raised a new alert at least four times, on 28 May – 8 June, on 20 June, on 4 July, and on 9-11 July. These were accompanied by significant increase in the SO<sub>2</sub> gas flux from the summit craters, and increase in the effusion rate that became twice the previous value with a delay of a few days (Fig. 10) causing the lava flow fronts to extend again to low elevations, as well as increase in the explosive activity and an increase in the effusion rate from the upper vents along the eruptive fissure. During this period, deep explosive activity started from the North-East Crater (NEC), figure 1, and an intense degassing produced a significant gas column from the pit at the eastern base of the SEC that was previously

obstructed by inner collapses. In the following month, the effusion rate progressively decreased. The eruption ended on 6 July 2009, after almost 14 months of continuous lava effusion.

## 5. Geophysical modeling of the intrusive process

On the morning of 13 May 2008, the continuous signals recorded at the permanent magnetic, tilt and GPS stations recorded significant changes during the intrusion [Napoli et al.; 2008; Aloisi et al., 2009]. Until 09:00 GMT, no significant changes were observed at all magnetic stations (Fig. 11, see Fig. 12 for names and codes of the stations). Soon after, large negative changes in the local magnetic field occurred at the stations set on the northern flank of the volcano within a few hours coinciding with the northward epicentral migration of the seismic events. The total intensity decreased by about 2.0 nT at PDN and 1.8 nT at PTL. Both sensors of PDG show the largest change among all the other sites. The total intensity of the magnetic field decreased more than 6.5 nT during the 5-hour period (from 9:00 to 14:00 GMT). The amount of the decrease fell off northward and no significant variations are observed at DGL. During the same period, the magnetic stations on the southern flank of the volcano showed minor variations. In particular, a negative change was detected at BVD (-1.8 nT), whereas the magnetic field at CST was almost unchanged. A slight positive variation of 1.8 nT was observed at BCN [Napoli et al., 2008]. The magnetic data clearly show a rapid change from 09:00 to 10:00 GMT, when most of the earthquakes (about 150 of 230) were recorded [Patanè, 2008]. Then, a decrease in the rate of magnetic variations was observed from 10:00 to 14:00 GMT during which a reduction in the earthquake rate was observed. After the seismic swarm ended, no further magnetic variations were detected at all stations [Napoli et al., 2008].

Very sharp tilt changes started first in the summit area where the largest variations (about 100 microradians) were detected from 8:40 at PDN station, which was the closest to the crater area, and tilt variations were successively observed in the middle flanks of the volcano, but with strong attenuation. MSC station, which is on the upper western flank (Fig. 12), recorded about 10 microradians; clear but

minor changes were recorded in the other stations on the middle flanks (Fig. 11). The summit stations of the continuous recording GPS network showed horizontal displacements of a few tens of centimeters. Smaller variations of a few centimeters were detected at the other stations. The deformation pattern was radial with respect to the summit area [Aloisi *et al.*, 2009].

Analytical solutions were used to model the geophysical observations and to infer the intrusion source parameters. Magnetic data inversion indicated the response to a tensile mechanism with an intrusion crossing the volcano edifice along a ca. NNW–SSE direction in the northern flank attributable to piezomagnetic effect (Fig. 12a). The estimated intrusive dike, located within the zone of the seismic swarm that occurred during magma propagation, generated a deformation pattern that also fits well the ground deformation recorded by the continuous GPS network operating on Mt Etna [Napoli *et al.*, 2008]. This analytical model provided a first acceptable representation of the magma intrusion by using a single intrusion source (Fig. 12a).

As also suggested by the temporal evolution of the seismic events and structural field evidence, an attempt to improve the source geometry was performed by Aloisi *et al.* [2009], who divided the intrusion into two phases (Fig. 12b, 12c). In particular, as suggested by the seismicity pattern and by the summit tilt gradient change, the intrusion time was divided into two intervals from 8:40 to 9:30 and from 9:30 to 17:00, which represent the phases of the ascending vertical dike-like intrusion and a following attempt of the magma to penetrate laterally towards the N, respectively. The first dike generated the intrusion in the high southern flank and the following eruptive fissure, while the lateral intrusion in the northern flank stopped without lava emission but induced a dry fracture field.

## **6. Simulation and prediction of the ash dispersal and lava flows**

### **6.1 Ash dispersal and fall-out simulation**

During the previous long-lasting explosive activity of the 2001 and 2002-2003 eruptions, the decisions of opening/closure of the air traffic were adopted following the decisions of ENAC, the

national organization for civil aviation. The final ENAC decisions lacked precise scientific evaluations and this has created problems and uncertainties.

As result of the 2006 eruption, characterized by a permanent high strombolian activity, the Italian Department of Civil Defence (DPC) and INGV planned to implement a surveillance system for both monitoring the ash dispersal of the explosive activity and for supporting the DPC's objectives and decisions. The INGV set up an ash surveillance system composed of monitoring, forecasting and validation. The ash monitoring of the explosive activity was controlled by signals from seismicity, seismic tremors and images from permanent visible and thermal cameras. Moreover, a further validation of the ongoing phenomena was obtained by the images from geostationary satellite (Meteosat).

The ash dispersion forecasting was performed by using the meteorological forecast data for the next 48 hours, received every morning from the Italian Air Force, and by running different air dispersal and fall-out models such as HAZMAP [Macedonio *et al.*, 2005], TEPHRA [Bonadonna *et al.*, 2005], FALL3D [Costa *et al.*, 2006] and PUFF [Searcy *et al.*, 1998]. All the models are continuously running at INGV in Catania, and the simulations are sent via internet to the Civil Protection Department that produces the '*hazard bulletin*' for the airports, which clearly defines the sectors affected by the ash fall-out and the risk level for the flights and the airport.

The surveillance system started up during the lava fountain episodes of 2007; it proved very helpful during the lava fountain that began in the late afternoon of September 4, 2007 and lasted about 12 hours. Despite the long duration of this episode, the simulation showed that the ash plume was clearly moving in the eastern direction during the following 48 hours with an elongated shape of the fall-out and without affecting the Catania airport. The hazard bulletins for aviation were very precise and the airport worked regularly without interruptions.

The start of the 2008 eruption was another important test-case to validate the importance of this surveillance system. The alert was made promptly at the beginning of the seismic swarm allowing the DPC to send the first hazard bulletin to the airport authorities. The bad weather conditions did not allow the permanent cameras to detect the explosive activity but, as shown in Section 3, the satellite

confirmed a plume moving towards the NE from 9:30. The ash dispersal simulation forecasted for the following 24 hours a well-shaped and stable plume elongating towards the NE without affecting the area around the Catania airport (Fig. 13). The precise information provided the first hazard bulletin with clear indications of the area affected by the ash dispersal, allowing the aviation and airport authorities to advise pilots so that they could use alternative flying routes, landing and taking off from the W rather than the E. The second hazard bulletin on the afternoon of 14 May communicated the end of the violent ash emission. During this time, the hazard bulletins allowed the Catania airport to be correctly informed of the ongoing phenomena and the plume cloud forecasting. The airport did not suffer interruptions and operated on a regular schedule.

## 6.2 Lava flow simulations

Between 13 May and 21 June 2008 we simulated the expansion of the lava flow field for hazard purposes every day using the MAGFLOW model [Vicari *et al.*, 2007; Del Negro *et al.*, 2008]. The data required to run MAGFLOW are : *i*) the digital elevation model (DEM), *ii*) the conditions for extrusion of lava, and *iii*) the physical and rheological properties of lava. However, for a given composition, the volumetric flux of lava from the vent (i.e. the lava effusion rate, Harris *et al.*, 2007; Harris and Baloga, 2009) is the principal parameter controlling the final flow dimensions. Direct field measurements of lava effusion rate are often difficult to make during the early phases of an eruption, especially when lava flows expand at high speed, and strong explosions, fountaining and lava spattering occur at or near the master vent [Pinkerton and Sparks, 1976; Frazzetta and Romano, 1984; Calvari *et al.*, 1994, 2003; Behncke and Neri, 2003a; Lautze *et al.*, 2004; Bailey *et al.*, 2006]. In all these cases, the timely synoptic view offered by satellite-based sensors can be used to estimate instantaneous lava flow output [Harris *et al.*, 1997a, 2000; Herault *et al.*, 2007; Harris and Baloga, 2009]. To this end, we implemented an automated system that uses infrared satellite data acquired by MODIS to estimate the time-averaged discharge rate following the methodology of Harris *et al.*, [1997a, 1997b, 1998].

The data set consists of about 90 cloud-free satellite images of the MODIS sensor of the TERRA and AQUA satellites. The sequence started on 13 May at 09:45 GMT. Figure 10 shows the estimated

values of effusion rate for the period from 13 May to 15 July 2008. The estimated satellite effusion rate values showed a fairly usual trend, at least for the first five days of the eruption. The maximum values of flow rate were reached between the first and the third day of eruption, then the effusion rate sharply decreased. After that, an increasing trend was observed in the second half of June, reaching peaks of about half of the initial highest values (Fig. 10). This is not common during dike drainage and suggests that new inputs of gas-rich magma entered the system [Calvari *et al.*, 2005a, 2005b, 2010], causing some concern for a possible greater expansion of the lava flows. For this reason, satellite-derived time-varying eruption rates were constantly used during the 2008 eruption every day as a basis to obtain numerical simulations of lava flow paths using the MAGFLOW Cellular Automata model [Herault *et al.*, 2009; Vicari *et al.*, 2009]. The physical and rheological parameters used for the simulations are reported in Table 1. As a topographic base, we have used the Digital Elevation Model (DEM) of Etna from data collected during the 2007 aerophotogrammetric flight that has a resolution of 10 meters. Since this DEM did not cover the entire area for our simulation, it was extended by using the 2005 topographic base, thanks to the contribution of INGV, Pisa.

Two vents V1 and V2 (Fig. 9), active on 13 May in the eastern part of the summit craters, were considered for numerical simulation. Indeed, the satellite-derived time-averaged discharge rates represent the total effusion rates from the two vents V1 and V2, so a critical parameter for the simulations is the relative weight of the flux rate for each vent. After several attempts of varying the allotting of flux rate between the two vents, the best results are shown in figure 14, where a 40 days extrusion interval is illustrated assigning 1/3 part of the total flux rate to V1 and 2/3 to V2. The simulated scenario reproduces the observed lava field well. Mismatching between the simulated and the observed path of lava flow in the northern branch is probably due to the influence on DEM used for the simulation by two 2007 lava fountains, 4 September and 23 November (Fig. 1). Starting from this base configuration of simulation parameters, several other simulations were performed during the early phase of the eruption in order to verify which conditions, especially for the values of the effusion rate, could be considered as a threshold of alert. For all simulated scenarios, no lava flow path extended



beyond the Valle del Bove area, even if high values of the effusion rates were used as input of MAGFLOW.

## 7. Discussion

Mt. Etna is characterized by a persistent degassing activity from the summit craters through which the magma residing in the upper conduit gradually releases its explosive power [Behncke *et al.*, 2005, and reference therein). Following Rittmann [1973], effusive eruptions at this volcano can be divided into four main classes: 1) *terminal eruptions*, or eruptions involving overflow of magma from the summit craters and accompanied or not by explosive activity (strombolian or fire fountains), which are the consequence of the extrusion of magma from a shallow reservoir through the central conduit of the volcano; 2) *subterminal eruptions*, involving the summit region above 3000 m elevation and thus the area immediately surrounding the summit craters; 3) *flank lateral eruptions* [or central-lateral eruptions according to Acocella and Neri, 2003], in which magma from the central conduit intrudes as lateral dikes and erupts on the volcano flanks, commonly characterized by multiple vents aligned along the eruptive fissure that radiates from the summit of the volcano [Bonaccorso and Davis, 2004] and by explosive activity during the initial phases of the eruption; and 4) *flank eccentric eruptions* [also named peripheral eruptions; Acocella and Neri, 2003], or eruptions triggered by dike-forming intrusion rising straight from the magma reservoir without using the central conduit, and that for this reason keep their original gas content until the start of the eruption, giving rise to extremely powerful and prolonged explosive phases, such as recently occurred in 1974, 2001, and 2002-2003 [Guest *et al.*, 1974; Behncke and Neri, 2003b; Lanzafame *et al.*, 2003; Andronico *et al.*, 2005; Neri *et al.*, 2005; Acocella and Neri, 2009].

The ground deformation modeling of the several flank eruptions occurring on Etna in the last three decades confirmed that the flank eruptions can be divided into the two classes : lateral and eccentric [see Bonaccorso and Davis, 2004 for a review]. The first type involves magma rising along

the upper central conduit system before breaking out into shallow dikes propagating horizontally. The second type involves dikes that are generated at depths of several km and expand vertically through the volcanic pile provoking marked deformation until they break the surface and erupt explosively without intersecting the central conduit.

The intrusion associated with the 2008-2009 eruption was characterized by a different mechanism, never observed or modeled before at Etna. In this case, as shown by magnetic and deformation modeling, the near-vertical intrusion departed from the central conduit system at a depth of 1.6 km below the summit area and propagated towards the E, without following the path of the central conduit (Fig. 15). This is neither a classic central-lateral eruption propagating radially from the upper portion of the conduit towards the volcano flanks, nor a classic eccentric eruption cutting the entire volcano pile. The diversion from the upper conduit of the propagating dike-forming intrusion could be triggered by the rapid rise of the significant volume of rich-gas magma erupted through the powerful lava fountain on 10 May 2008, only three days before beginning of the 2008-2009 flank eruption. The overpressure of magma in the SEC conduit could have caused fracturing around the conduit itself at ~1.6 km of depth, facilitating three days later (on 13 May) the intrusion of a dike out of the conduit, in a NE direction. Therefore, we believe that the accumulation of gas-rich magma at shallow depth (~1.6 km) maintained its eruptive power, and also triggered the flank eruption three days later. The shallow depth of the departure of the intrusion below the summit area (~1.6 km), which corresponds to the centroid depth of the source of the volcanic tremor (Fig. 7b), was inferred by the deformation that was restricted to the summit area.

The initial phase of the eruption raised two main hazards, namely the ash dispersal produced by the explosive activity and the magma fracture propagation towards the N. A third critical hazard was related to the high effusion rate during this initial phase and its increase measured by satellite (28 May – 8 June, 20 June, 4 July, and 9-11 July), and associated with augmented seismic tremor, that could have resulted in a greater growth of the lava flow field.

As described in the previous Section 6.1, this was the first instance during an eruption of the complete monitoring application of the surveillance system developed by INGV for the ash clouds

detection and simulation. The interaction with the Italian DPC was very effective and the precise information provided by the hazard bulletin permitted a timely management of this hazard without the unnecessary closure of the Catania airport [Calvari *et al.*, 2001; Andronico *et al.*, 2005].

During the first days, there was great concern for the possible eruptive fissure propagation towards the N. In fact, as inferred by seismicity during the intrusive phase (Fig. 6) and by ground deformation modeling (Fig. 12b1, 12b2), the dike-forming intrusion moved towards the N along its shallower part. This attempt to penetrate the N flank was confirmed by the field structural investigation that revealed ~N-S dry fractures propagating along the upper sector of the NE Rift (Fig. 9). The concern was particularly high because similar fractures opened during the first phase of the 1981 eruption, when in a few hours the lavas destroyed about 1 km of railway, several roads and other infrastructures, and approached the town of Randazzo. On that occasion, an eccentric magma fracture vertically crossed the entire volcanic edifice and caused significant deformation of the entire volcano edifice [Bonaccorso, 1999]. Contrary to the expected, this time the limited ground deformation pattern recorded during 13 May 2008 argued against this dangerous situation.

The lateral propagation of the dike-forming fracture towards the N was probably halted by the moderate volume of the intrusion, by the shallow origin of the dike (~1600 m with respect to the surface, Fig. 15) and by the reduction of pressure due to the concomitant eruption with magma drainage along the SE portion of the dike inside the Valle del Bove [Aloisi *et al.*, 2009]. During its northern propagation, the 2008 intrusion moved towards the NEC conduit (Fig. 9) but without triggering any visible eruptive activity from this summit crater. This reveals that the origin of the 2008 dike was linked to the shallow storage of the SEC conduit, although at the surface the position of the eruptive and dry fissures was closer to the NEC (Fig. 15). The structural field investigation suggested that the NNW extremity of the magmatic intrusion was confined to about 800 meters below the topographic surface, causing the opening of a ~N-S dry, 2450 m long and 200-800 m wide asymmetric graben (Fig. 9). The ~N-S dry fractures thus formed and expanded until the first lava flow was erupted from the surface fissure that opened towards the S and SE into the Valle del Bove. The sharply declining effusion rate of

this first phase of the eruption (Fig. 10) is typical of dike drainage, as already described by *Wadge* [1977] and *Harris et al.* [2000].

The last major hazard was posed by lava flows and the possibility that, depending on the increased effusion rate, the lava could extend beyond the Valle del Bove depression and threaten the infrastructures and villages on the eastern flank. Indeed, a higher and steady lava supply as observed after mid May 2008 (Fig. 10) could have resulted in lava tube growth, thus lengthening the lava flow field much more than in cases of channel-fed flows [see *Calvari et al.*, 1994; *Calvari and Pinkerton*, 1998; 1999]. This is why particular attention was given to the daily calculation of effusion rate and the simulation of lava flow spreading and the information promptly forwarded to DPC. The thermal state and effusion rate of the 2008 Etna eruption have been monitored by an automatic system that uses satellite data with different refresh times as input. The system was able to observe short dynamic activities such as the lava fountain preceding the eruption and to follow the different phases of the eruptive activity. It also provides a tool that can assess the hazard posed by hypothetical and ongoing eruptions. During the following stage, from the end of May to mid July, even if the lava was continuously erupted from the eruptive fissure, we did not observe any gradual decline in effusion rate. On the contrary, in the second part of July 2008, some phases of increased effusion rate were recorded (Fig. 10). The associated sudden increase in volcanic tremor, gas release, and effusion rate indicated a new input of gas-rich magma within the system. This process happened at least four times during the initial phase of the 2008-2009 eruption here described, suggesting new inputs of gas-rich magma within the shallow magma storage region of the volcano [*Calvari et al.*, 2005a, 2005b, 2010]. With time, increasingly smaller gas-rich magma pockets entered the system, as revealed by the shorter duration of the explosive phase and the decline in effusion rate, thus significantly decreasing the hazard posed by the eruption.

## **Conclusion**

The results presented here show how a potentially dramatic eruption occurring in a densely populated area and close to the third largest international airport of Italy has been managed without significant economic damage, providing an effective evaluation of the posed hazards and the correct forecast scenarios. We have highlighted the great benefit of continuous feedback between research and monitoring, as well as the importance of integrated multi-disciplinary monitoring networks and techniques when dealing with a magmatic intrusion that can suddenly change its path at depth. In particular, volcanic tremor localization and ground deformation modeling allowed interpreting the mechanisms of the final intrusive process and the shape of the feeder dike. The interpretation of the deformation field excluded further dike propagation towards the lower flank of the N sector, in contrast with the devastation that occurred during the 1981 eruption.

During the explosive phase, ash spreading in the atmosphere could have raised concern and produced disruption to the international airport at Catania, as occurred in 2001 and 2002. However, the continuous monitoring of the eruptive cloud, coupled with the application of several software packages for ash spreading simulations and then integrated with wind forecasting, and especially the routine established between Istituto Nazionale di Geofisica e Vulcanologia, the Italian Civil Defense Department and the Italian National Organization for Civil Aviation, resulted in an eruption that proceeded with minimal impact from an economic point of view, without interrupting the regional air traffic. Once the eruption started, it was essential to obtain daily measurements of effusion rates from satellites and forecast lava flow spreading. In fact, the effusion rate peaks observed after May 2008, accompanied by increasing seismic tremor and gas output from the summit craters, revealed new inputs of gas-rich magma entering the supply system. This resulted in a greater down slope extension of the lava flows that reached lower elevations, raising concern for the possibility of tube development within the lava flow field, thus accreting even more the potential of longer flows. However, daily calculations of the effusion rate from satellite and immediate lava flow simulations using the MAGFLOW model have allowed us to keep our estimates of the expansion of the lava flow field up to date and accurate.

This multi-disciplinary approach prompted an efficient feedback between monitoring and research, which is very helpful for an effective support to risk evaluation.

## References

- Acocella, V., and M. Neri (2003), What makes flank eruptions? The 2001 Etna eruption and the possible triggering mechanisms, *Bull. Volc.*, *65*, 517-529, doi: 10.1007/s00445-003-0280-3.
- Acocella, V., and M. Neri (2009), Dike propagation in volcanic edifices: overview and possible developments, Special Issue: Gudmundsson – Volcanoes, *Tectonophysics*, *471*, 67-77, doi: 10.1016/j.tecto.2008.10.002.
- Allard, P., B. Behncke, S. D'Amico, M. Neri, and S. Gambino (2006), Mount Etna 1993–2005: Anatomy of an evolving eruptive cycle, *Earth-Science Reviews*, *78*, 85-114.
- Aloisi, M., A. Bonaccorso, F. Cannavò, S. Gambino, M. Mattia, G. Puglisi, and E. Boschi (2009), A new dike intrusion style for the Mount Etna May 2008 eruption modelled through continuous tilt and GPS data, *Terra Nova*, *21*, 4, 316-321.
- Andronico, D., S. Branca, S. Calvari, M.R. Burton, T. Caltabiano, R.A. Corsaro, P. Del Carlo, G. Garfi, L. Lodato, L. Miraglia, F. Muré, M. Neri, E. Pecora, M. Pompilio, G. Salerno, and L. Spampinato (2005), A multi-disciplinary study of the 2002-03 Etna eruption: insights into a complex plumbing system, *Bull. Volc.*, *67*, 314-330, doi:10.1007/s00445-004-0372-8.
- Andronico, D., S. Scollo, A. Cristaldi, and F. Ferrari (2009), Monitoring ash emission episodes at Mt. Etna: The 16 November 2006 case study, *J. Volc. Geoth. Res.*, *180*, 123-134.
- Bailey, J. E., A. J. L. Harris, J. Dehn, S. Calvari, and S. K. Rowland (2006), The changing morphology of an open lava channel on Mt. Etna, *Bull. Volc.*, *68*(6), 497–515, doi:10.1007/s00445-005-0025-6.
- Barberi, F., M. L. Carapezza, M. Valenza, and L. Villari (1993), The control of lava flow during the 1991-1992 eruption of Mt. Etna, , *J. Volc. Geoth. Res.*, *56*, 1-34.
- Barberi, F., F. Brondi, M.L. Carapezza, L. Cavarra, C. Murgia (2003), Earthen barriers to control lava flows in the 2001 eruption of Mt. Etna, *J. Volc. Geoth. Res.*, *123*, 231-243.
- Battaglia, J., K. Aki, and V. Ferrazzini (2005), Location of tremor sources and estimation of lava output using tremor source amplitude on the Piton de la Fournaise volcano: 1. Location of tremor sources, *J. Volc. Geoth. Res.*, *147*, 268-290.
- Behncke, B., and S. Calvari (2008), Etna: 6-km-long lava flow; ash emissions; 13 May 2008 opening of a new eruptive fissure. *Bull. Global Volc. Network*, *33* (5), 11-15.

- Behncke, B., and M. Neri (2003a), Cycles and trends in the recent eruptive behaviour of Mount Etna (Italy), *Can. J. Earth Sci.*, *40*, 1405-1411, doi: 10.1139/E03-052.
- Behncke, B. and M. Neri (2003b), The July-August 2001 eruption of Mt. Etna (Sicily), *Bull. Volcanol.*, *65*, 461-476, doi: 10.1007/s00445-003-0274-1.
- Behncke, B., M. Neri, and A. Nagay (2005), Lava flow hazard at Mount Etna (Italy): New data from a GIS-based study, in *Kinematics and dynamics of lava flows*, edited by M. Manga, and G. Ventura, *Geol. Soc. Am. Spec. Pap.* *396*, 187-205, doi: 10.1130/0-8137-2396-5.189.
- Behncke, B., S. Calvari, S. Giammanco, M. Neri, and H. Pinkerton (2008), Pyroclastic density currents resulting from the interaction of basaltic magma with hydrothermally altered rock: an example from the 2006 summit eruptions of Mount Etna, Italy, *Bull. Volc.*, *70*, 1249–1268, doi:10.1007/s00445-008-0200-7.
- Behncke, B., S. Falsaperla, and E. Pecora (2009), Complex magma dynamics at Mount Etna revealed by seismic, thermal, and volcanological data, *J. Geophys. Res.*, *114*, B03211, doi:10.1029/2008JB005882.
- Billi, A., V. Acocella, R. Funicello, G. Giordano, G. Lanzafame, and M. Neri (2003), Mechanisms for ground-surface fracturing and incipient slope failure associated to the July-August 2001 eruption of Mt. Etna, Italy: analysis of ephemeral field data, *J. Volc. Geoth. Res.*, *122*, 3-4, 281-294.
- Bonaccorso, A. (1999), The March 1981 Mt. Etna eruption inferred through ground deformation modelling, *Phys. Earth Plan. Int.*, *112*, 125-136.
- Bonaccorso, A., and P.M. Davis (2004), Modeling of ground deformation associated with recent lateral eruptions: Mechanics of magma ascent and intermediate storage at Mt. Etna, in *Etna: Volcano Laboratory*, edited by A. Bonaccorso et al., *AGU Geophysical Monograph Series*, *143*, 293-306.
- Bonaccorso, A., S. Calvari, M. Coltelli, C. Del Negro, and S. Falsaperla Eds (2004a), Etna Volcano Laboratory, Geophysical Monograph series of *American Geophysical Union*, n.143, 369 pp.
- Bonaccorso, A., O. Campisi, G. Falzone, and S. Gambino (2004b), Continuous tilt monitoring: a lesson from 20 years experience at Mt. Etna, in *Etna: Volcano Laboratory*, edited by A. Bonaccorso et al., *AGU Geophysical Monograph Series*, *143*, 307-320.
- Bonaccorso, A., S. Cianetti, C. Giunchi, E. Transatti, M. Bonafede, and E. Boschi (2005), Analytical and 3D numerical modeling of Mt. Etna (Italy) volcano inflation, *Geophys. J. Int.*, *163*, 852-862.
- Bonaccorso, A., A. Bonforte, F. Guglielmino, M. Palano, G. Puglisi (2006), Composite ground deformation pattern forerunning the 2004–2005 Mount Etna eruption, *J. Geophys. Res.*, *111*, B12207, doi:10.1029/2005JB004206.

- Bonadonna, C., C.B. Connor, B.F. Houghton, L. Connor, M. Byrne, A. Laing, and T.K. Hincks (2005), Probabilistic modelling of tephra-fall dispersal: Hazard assessment of a multiphase rhyolitic eruption at Tarawera, New Zealand, *J. Geophys. Res.*, *110* (B3) 3203 doi:[10.1029/2003JB002896](https://doi.org/10.1029/2003JB002896).
- Bonforte, A., A. Bonaccorso, F. Guglielmino, M. Palano, G. Puglisi (2008), Feeding system and magma storage beneath Mt. Etna as revealed by recent inflation/deflation cycles, *J. Geophys. Res.*, *113*, B05406, doi:[10.1029/2007JB005334](https://doi.org/10.1029/2007JB005334).
- Bonforte, A., S. Gambino, F. Guglielmino, F. Obrizzo, M. Palano, and G. Puglisi (2007), Ground deformation modeling of flank dynamics prior to the 2002 eruption of Mt. Etna, *Bull. Volc.*, *69*, 757-768, doi:[10.1007/s00445-006-0106-1](https://doi.org/10.1007/s00445-006-0106-1).
- Bonforte, A., S. Gambino, and M. Neri (2009), Intrusion of eccentric dikes: The case of the 2001 eruption and its role, in *The dynamics of Mt. Etna volcano, Special Issue, Volcanoes, Tectonophysics*, *471*, 78-86, doi:[10.1016/j.tecto.2008.09.028](https://doi.org/10.1016/j.tecto.2008.09.028).
- Bonforte, A. and G. Puglisi (2006), Dynamics of the eastern flank of Mt. Etna volcano (Italy) investigated by a dense GPS network, *J. Volc. Geoth. Res.*, *153*, 357-369.
- Branca, S., and P. Del Carlo (2004), Eruptions of Mt Etna during the past 3,200 years: a revised compilation integrating the historical and stratigraphic records, in *Etna: Volcano Laboratory*, edited by A. Bonaccorso et al., *AGU Geophysical Monograph Series*, *143*, 1-27.
- Burton, M., M. Neri, D. Andronico, S. Branca, T. Caltabiano, S. Calvari, R.A. Corsaro, P. Del Carlo, G. Lanzafame, L. Lodato, L. Miraglia, F. Muré, G. Salerno, and L. Spampinato (2005), Etna 2004-05: an archetype for geodynamically-controlled effusive eruptions, *Geophys. Res. Lett.*, *32*, L09303, doi:[10.1029/2005GL022527](https://doi.org/10.1029/2005GL022527).
- Calvari, S., M. Coltelli, M. Neri, M. Pompilio, and V. Scribano (1994), The 1991-93 Etna eruption: chronology and lava flow field evolution, *Acta Vulcanologica*, *4*, 1-14.
- Calvari, S., and H. Pinkerton (1998), Formation of lava tubes and extensive flow field during the 1991-93 eruption of Mount Etna, *J. Geophys. Res.*, *103*(B11), 27,291-27,302, doi:[10.1029/97JB03388](https://doi.org/10.1029/97JB03388).
- Calvari, S., and H. Pinkerton (1999), Lava tube morphology on Etna and evidence for lava flow emplacement mechanisms, *J. Volc. Geoth. Res.*, *90*, 263-280.
- Calvari, S., and the whole scientific staff of INGV – Sezione di Catania (2001), Multidisciplinary Approach Yields Insight into Mt. Etna 2001 Eruption, *EOS Transactions*, *82*, (52), 653-656.



- Calvari, S., M. Neri, and H. Pinkerton (2003), Effusion rate estimations during the 1999 summit eruption on Mt. Etna, and growth of two distinct lava flow fields, *J. Volc. Geoth. Res.*, *119*, 107–123, doi:10.1016/S0377-200273(02)00308-6.
- Calvari, S., L. Spampinato, L. Lodato, A. J. L. Harris, M. R. Patrick, J. Dehn, M. R. Burton, and D. Andronico (2005a), Chronology and complex volcanic processes during the 2002–2003 flank eruption at Stromboli volcano (Italy) reconstructed from direct observations and surveys with a handheld thermal camera, *J. Geophys. Res.*, *110*, B02201, doi:10.1029/2004JB003129.
- Calvari, S., L. Spampinato, L. Lodato, A. J. L. Harris, M. R. Patrick, J. Dehn, M. R. Burton, and D. Andronico (2005b), Correction to “Chronology and Complex Volcanic Processes During the 2002–2003 Flank Eruption at Stromboli Volcano (Italy) Reconstructed From Direct Observations and Surveys With a Handheld Thermal Camera,” *J. Geophys. Res.*, *110*, B02201, doi:10.1029/2004JB003129.
- Calvari, S., L. Lodato, A. Steffke, A. Cristaldi, A.J.L. Harris, L. Spampinato, and E. Boschi (2010), The 2007 Stromboli eruption: Event chronology and effusion rates using thermal infrared data, *J. Geophys. Res.*, *115*, B4, B04201, doi:10.1029/2009JB006478.
- Costa, A., G. Macedonio, and A. Folch (2006), A three-dimensional Eulerian model for transport and deposition of volcanic ashes, *Earth Planet. Sci. Lett.*, *241*, 634–647.
- Day, S.J., J.C. Carracedo, H. Guillou, P. Gravestock (1999), Recent structural evolution of the Cumbre Vieja volcano, La Palma, Canary Islands: volcanic rift zone reconfiguration as a precursor to volcano flank instability? *J. Volc. Geoth. Res.*, *94*, 135-167.
- Del Negro, C., L. Fortuna, A. Herault, and A. Vicari (2008), Simulations of the 2004 lava flow at Etna volcano by the magflow Cellular Automata model, *Bull. Volc.*, *70*, 7, 805-812, doi: 10.1007/s00445-007-0168-
- Di Grazia, G., A. Cannata, P. Montalto, D. Patanè, E. Privitera, L. Zuccarello, and E. Boschi (2009), A multiparameter approach to volcano monitoring based on 4D analyses of seismo-volcanic and acoustic signals: The 2008 Mt. Etna eruption, *Geophys. Res. Lett.*, *36*, L18307, doi:10.1029/2009GL039567.
- Di Grazia, G., S. Falsaperla, and H. Langer (2006), Volcanic tremor location during the 2004 Mount Etna lava effusion, *Geophys. Res. Lett.*, *33*, L04304, doi:10.1029/2005GL025177.
- Frazzetta, G., and R. Romano (1984), The 1983 Etna Eruption: Event Chronology and Morphological Evolution of the Lava Flow, *Bull Volcanol*, *47*, 1079-1096.
- Gottschammer, E., and I. Surono (2000), Locating tremor and shock sources recorded at Bromo volcano. *J. Volc. Geoth. Res.*, *101*, 199-209.

- Gresta, S., V. Longo, and A. Viavattene (1990), Geodynamic behaviour of eastern and western sides of Mount Etna, *Tectonophysics*, *179*, 81-92.
- Guest, J.E., A.T. Huntingdon, G. Wadge, J.L. Brander, B. Booth, S. Carter, and A. Duncan (1974), Recent eruption of Mount Etna, *Nature*, *250*, 385-387.
- Harris, A. J. L., and S. M. Baloga (2009), Lava discharge rates from satellite-measured heat flux, *Geophys. Res. Lett.*, *36*, L19302, doi:10.1029/2009GL039717.
- Harris, A. J. L., A. L. Butterworth, R. W. Carlton, I. Downey, P. Miller, P. Navarro, and D. A. Rothery (1997a), Low-cost volcano surveillance from space: Case studies from Etna, Krafla, Cerro Negro, Fogo, Lascar and Erebus. *Bull. Volc.*, *59*, 49–64, doi:10.1007/s004450050174.
- Harris, A.J.L., S. Blake, D.A. Rothery, and N.F Stevens (1997b), A chronology of the 1991 to 1993 Mount Etna eruption using advanced very high resolution radiometer data: Implications for real-time thermal volcano monitoring, *J. Geophys. Res.*, *102* (B4), 7985-8003.
- Harris, A.J.L., L.P. Flynn, L. Keszthelyi, P.J. Mougini-Mark, S.K. Rowland, and J.A. Resing (1998), Calculation of lava effusion rates from Landsat TM data, *Bull. Volc.*, *60*, 52-71.
- Harris, A. J. L., J. B. Murray, S. E. Aries, M. A. Davies, L. P. Flynn, M. J. Wooster, R. Wright, and D. A. Rothery (2000), Effusion rate trends at Etna and Krafla and their implications for eruptive mechanisms, *J. Volc. Geoth. Res.*, *102*, 237–270, doi:10.1016/S0377-0273(00)00190-6.
- Harris, A., D. Pirie, K. Horton, H. Garbeil, E. Pilger, H. Ramm, R. Hoblitt, C. Thornber, M. Ripepe, E. Marchetti, and P. Poggi (2005), DUCKS: Low cost thermal monitoring units for near-vent deployment, *J. Volc. Geoth. Res.*, *143*, 335-360, doi:10.1016/j.jvolgeores.2004.12.007.
- Harris, A. J. L., J. Dehn, and S. Calvari (2007), Lava effusion rate definition, measurement and operational requirements: A review, *Bull. Volc.*, *70*, 1–22, doi:10.1007/s00445-007-0120-y.
- Herault, A., A. Vicari, A. Cirauco, and C. Del Negro (2009), Forecasting Lava Flow Hazard During the 2006 Etna Eruption: Using the Magflow Cellular Automata Model, *Comput. Geosci.*, doi:10.1016/j.cageo.2007.10.008
- Lanzafame, G., M. Neri, V. Acocella, A. Billi, R. Funicello and G. Giordano (2003), Structural features of the July-August 2001 Mount Etna eruption: evidence for a complex magma supply system, *J. Geol. Soc. London*, *160*, 531-544, doi: 10.1144/0016-764902-151.

- Lautze, N.C., A.J.L. Harris, J.E. Bailey, M. Ripepe, S. Calvari, J. Dehn, S. Rowland, and K. Evans-Jones (2004), Pulsed lava effusion at Mount Etna during 2001, *J. Volc. Geoth. Res.*, *137*, 231-246, DOI: 10.1016/j.jvolgeores.2004.05.018.
- Macedonio, G., A. Costa, and A. Longo (2005), A computer model for volcanic ash fallout and assessment of subsequent hazard, *Comput. Geosci.*, *31*, 837–845.
- McGuire, W.J., J.B. Murray, A.D. Pullen, and S.J. Saunders (1991), Ground deformation monitoring at Mt. Etna: evidence for dyke emplacement and slope instability, *J. Geol. Soc. London*, *148*, 577-583.
- Napoli, R., G. Currenti, C. Del Negro, F. Greco and D. Scandura (2008), Volcanomagnetic evidence of the magmatic intrusion on 13th May 2008 Etna eruption, *Geophys. Res. Lett.*, *35*, L22301, doi:10.1029/2008GL035350.
- Neri, M., and V. Acocella (2006), The 2004-05 Etna eruption: implications for flank deformation and structural behaviour of the volcano. *J. Volc. Geoth. Res.*, *158*, 195-206, doi:10.1016/j.jvolgeores.2006.04.022.
- Neri, M., V. Acocella and B. Behncke (2004), The role of the Pernicana Fault System in the spreading of Mount Etna (Italy) during the 2002-2003 eruption. *Bull. Volcanol.*, *66*, 417-430, doi: 10.1007/s00445-003-0322-x.
- Neri, M., V. Acocella, B. Behncke, V. Maiolino, A. Ursino, and R. Velardita (2005), Contrasting triggering mechanisms of the 2001 and 2002-2003 eruptions of Mount Etna (Italy). *J. Volc. Geoth. Res.*, *144*, 235-255, doi:10.1016/j.jvolgeores.2004.11.025.
- Neri M., B. Behncke, M. Burton, S. Giammanco, E. Pecora, E. Privitera, and D. Reitano (2006), Continuous soil radon monitoring during the July 2006 Etna eruption, *Geophys. Res. Lett.*, *33*, L24316, doi:10.1029/2006GL028394.
- Neri, M., F. Mazzarini, S. Tarquini, M. Bisson, I. Isola, and B. Behncke (2008), The changing face of Mount Etna's summit area documented with Lidar technology. *Geophys. Res. Lett.*, *35*, L09305, doi:10.1029/2008GL033740.
- Neri, M., F. Casu, V. Acocella, G. Solaro, S. Pepe, P. Berardino, E. Sansosti, T. Caltabiano, P. Lundgren, R. Lanari (2009), Deformation and eruptions at Mt. Etna (Italy): a lesson from 15 years of observations. *Geophys. Res. Lett.*, *36*, L02309, doi:10.1029/2008GL036151.
- Patanè, D. (2008), Quadro di sintesi e aggiornamento al 19 Maggio 2008 sullo stato di attività sismica dell'Etna, INGV-CT internal report WKRSM20080519, at <http://www.ct.ingv.it/Etna2007/main.htm>
- Pinkerton, H., and R.S.J. Sparks (1976), The 1975 subterminal lavas, Mount Etna: A case history of the formation of a compound lava field, *J. Volc. Geoth. Res.*, *1*, 167-182.
- Pollard, D.D., P.T. Delaney, W.A. Duedl, E.T. Endo, and E.T. Okamura (1983), Surface deformation in volcanic rift zones, *Tectonophysics*, *94*, 541-584.

- Puglisi, G., and A. Bonforte (2004), Dynamics of Mount Etna Volcano inferred from static and kinematic GPS measurements, *J. Geophys. Res.*, *109* (B11), B11404, doi:10.1029/2003JB002878.
- Puglisi, G., A. Bonforte, A. Ferretti, F. Guglielmino, M. Palano, and C. Prati (2008), Dynamics of Mount Etna before, during, and after the July–August 2001 eruption inferred from GPS and differential synthetic aperture radar interferometry data, *J. Geophys. Res.*, *113*, B06405, doi:10.1029/2006JB004811.
- Rittmann, A. (1973), Structure and evolution of Mount Etna, *Phil. Trans. R. Soc. London*, *274 A*, 5-16.
- Roberts, G., M.J. Wooster, G.L.W. Perry, N. Drake, L.-M. Rebelo, and F. Dipotso (2005), Retrieval of biomass combustion rates and totals from fire radiative power observations: Application to southern Africa using geostationary SEVIRI imagery, *J. Geophys. Res.*, *110*, D21111, doi:10.1029/2005JD006018
- Ruch, J., V. Acocella, F. Storti, M. Neri, S. Pepe, G. Solaro, E. Sansosti (2010), Detachment depth of an unstable volcano revealed by rollover deformation: an integrated approach at Mt. Etna, *Geophys. Res. Lett.*, *37*, LXXXXX, doi:10.1029/2010GL044131.
- Rust, D., B. Behncke, M. Neri, and A. Ciocanel (2005), Nested zones of instability in the Mount Etna volcanic edifice, Sicily, *J. Volc. Geoth. Res.*, *144*, 137-153, doi: 10.1016/j.jvolgeores.2004.11.021.
- Searcy, C., K. Dean, and W. Stringer (1998), PUFF: A high-resolution volcanic ash tracking model, *J. Volc. Geoth. Res.*, *80*, 1–16.
- Solaro, G., V. Acocella, S. Pepe, J. Ruch, M. Neri, and E. Sansosti (2010), Anatomy of an unstable volcano through InSAR data: multiple processes affecting flank instability at Mt. Etna in 1994-2008, *J. Geophys. Res.*, doi:10.1029/2009JB000820, in press.
- Stevens, N.F., J.B. Murray, and G. Wadge (1997), The volume and shape of the 1991-1993 lava flow field at Mount Etna, Sicily, *Bull. Volc.*, *58*, 449-454.
- Vicari, A., A. Herault, C. Del Negro, M. Coltelli, M. Marsella, and C. Proietti (2007), Modelling of the 2001 Lava Flow at Etna Volcano by a Cellular Automata Approach, *Env. Modelling & Software*, *22*, 1465-1471.
- Vicari, A., A. Cirauda, C. Del Negro, A. Herault, and L. Fortuna (2009), Lava flow simulations using effusion rates from thermal infrared satellite imagery during the 2006 Etna eruption, *Natural Hazard*, doi:10.1007/s11069-008-9306-7.
- Wadge, G. (1977), The storage and release of magma on Mount Etna, *J. Volc. Geoth. Res.*, *2*, 361-384.
- Walter, T.R., V. Acocella, M. Neri, and F. Amelung (2005), Feedback processes between magmatism and E-flank movement at Mt. Etna (Italy) during the 2002-2003 eruption, *J. Geophys. Res.*, *110*, B10205, doi:10.1029/2005JB003688.

## **Acknowledgements**

We wish to thank all our colleagues from INGV Sezione di Catania for data collection, for the maintenance of the monitoring networks during the whole eruption, and for the many discussions about the interpretation of the eruptive events; the Etna Guides, the Funivia dell'Etna, and especially Alfio Mazzaglia and Nino Mazzaglia, for the prompt information pertaining any news about the summit eruptive activity at Mt. Etna; the Italian Civil Defence (DPC), for the close and efficient collaboration built up during the last height years of activity at Etna and other Sicilian volcanoes.

We are indebted to Paul Davis for his positive and encouraging comments. We thank the Associate Editor Michael P. Ryan, who helped greatly in improving the form of the manuscript. This study was undertaken with partial financial support from the INGV-DPC 2007–2009 Agreement. Scientific papers funded by DPC do not represent its official opinion and politics. We thank Stephen Conway for revising the English language of this manuscript.

## FIGURE and TABLE CAPTIONS

**Figure 1** – Etna map with the lava flows of the 2001-2007 flank eruptions. VOR=Voragine; BN=Bocca Nuova; NEC=North-East Crater; SEC=Couth-East Crater. Inset (a) detail of the summit craters area upgraded in June 2007 [from *Neri et al.*, 2008]. Inset (b) extent of the unstable sectors (1) of Mt. Etna; (2) the assumed off-shore boundary of the spreading area; (3) the directions of movement of the sliding sectors; and (4) boundaries of the sliding sectors to the North (Pernicana Fault system - PFS) and to the S-W (Ragalna Fault System - RFS).

**Figure 2** – Example of deflation/inflation cycles : a) deflation accompanying the 2004 eruption, b) inflation preceding the 2006 eruption, c) deflation accompanying the 2006 eruption, d) inflation preceding the 2008 eruption.

**Figure 3** - The Mt. Etna seismicity from January 2007 to May 2008: a) epicentral map; b) E-W cross section (the black circles indicate the events of the 13 May 2008 co-eruptive swarm). All the epicenters of the map are reported in the E-W cross section; c) strain release and earthquake daily rate (the dashed line marks the acceleration in the seismic energy release from January 2008 till the eruption; the two arrows, from left to right, indicate the deep swarm on January 7, 2008 and the co-eruptive swarm, respectively).

**Figure 4** – Photo of the 10 May 2008 explosive activity taken from the southern flank looking northwards at 1800 m asl altitude.

**Figure 5**– Radiative Power during 10 May 2008 lava fountain by SEVIRI data. On the top, three instants are reported on Google Map service: the beginning (a - top left map, green dot in the plot); the strongest phase (b - top middle map, blue dot in the plot); the decreasing phase (c - top left map, yellow-orange dot in the plot).

**Figure 6** – Location of the seismic swarm preceding and accompanying the onset of eruption on 13 May 2008 plotted as function of latitude vs. time. The size of the circles is proportional to the duration magnitude ( $M_{Dmin} = 1.0$ ,  $M_{Dmax} = 3.3$ ). The line is a fourth order polynomial curve fitting the dataset. In the inset is shown the map of the summit area with the position of the epicenters.

**Figure 7** – Volcanic tremor from 1 May 2008 to 13 May 2008: a) epicentral map of the source tremor locations; b) E-W cross section; c) tremor amplitude. The red dots refer to events recorded on 13 May from 06:40 GMT, in concomitance with the first significant variations in tremor amplitude and location preceding the onset of the eruption. The tremor amplitude sharp increase on 10 May is relative to the lava fountaining episode.

**Figure 8** - SEVIRI channel 4 calibrated radiance acquired during 13 May 2008. Yellow pixels are associated with the radiation from the ash plume, while red pixels are thermally anomalous.

**Figure 9** - Detailed map of the fracture field formed on 13 May 2008. The inset diagrams show the strike of the eruptive (a1 and a2) and dry (b) fractures.

**Figure 10** - Mean effusion rate values obtained from MODIS satellite images for the period 13 May - 16 July 2008. Spread in the data, calculated as difference between maximum and minimum value of effusion rate, is indicated for each point as a vertical bar. Note the initial fast decline in effusion rate, and the increase in activity during June. See text for further details.

**Figure 11** - Continuous magnetic (on the left) and tilt (on the right) signals during 13 May 2010 eruption. Daily mean differences of total magnetic intensity with respect to CSR station in May 2008 (top on the left). A daily mobile averaging with an overlapping window of 2 h is performed on magnetic data recorded in May to remove diurnal components. Ten-minute means of total intensity

variations on 13 May 2008 after removing diurnal components using notch filter centered at 8, 12, and 24 h (bottom on the left). The permanent tilt network comprises nine bi-axial instruments installed in shallow boreholes at about 3 m depth, and one long-base instrument at PDN [for details see *Bonaccorso et al.*, 2004b]. The radial axis of each tiltmeter is directed toward the Voragine crater, and a positive signal variation means crater-up tilting.

**Figure 12** – Dike modeling : a) magnetic data modeling [redrawn from *Napoli et al.*, 2008]; b1) GPS and tilt modeling of the first intrusion phase from 8:40 to 9:30 GMT, b2) GPS and tilt modeling of the second intrusion phase from 9:40 to 17:30 GMT [redrawn from *Aloisi et al.*, 2009]. Piezomagnetic anomaly has the contour lines at 1 nT. The epicenters of the most energetic seismic events are shown with circles [after *Napoli et al.*, 2008]. The red circles are the seismic events in correspondence of the step-like magnetic changes. The coordinates are in UTM projection, zone 33 N.

**Figure 13** - Volcano ash dispersal forecasting at 3000 m asl between 09:00 and 12:00 GMT of 13 May 2010 by using FALL3-D model [*Costa et al.*, 2006]. Image elaborated from INGV-CT and sent to Civil Defense Department.

**Figure 14** - Lava flow simulation using MAGFLOW model for the first forty days of eruption. V1 and V2 are the two effusive vents. Colored scale represents the lava flow thickness. The blue contour line is the observed lava flow field at June 21 2008 [*Bencke and Calvari*, 2008].

**Figure 15** – 3-D block diagram of Mt. Etna (looking W) illustrating the storage areas feeding the South-East Crater (SEC). After the violent lava fountaining on 10 May 2008, a diverging dike formed on the morning of 13 May immediately above the shallow storage. This corresponds to the source of the volcanic tremor and explains why deformation was restricted to the summit area. The magma

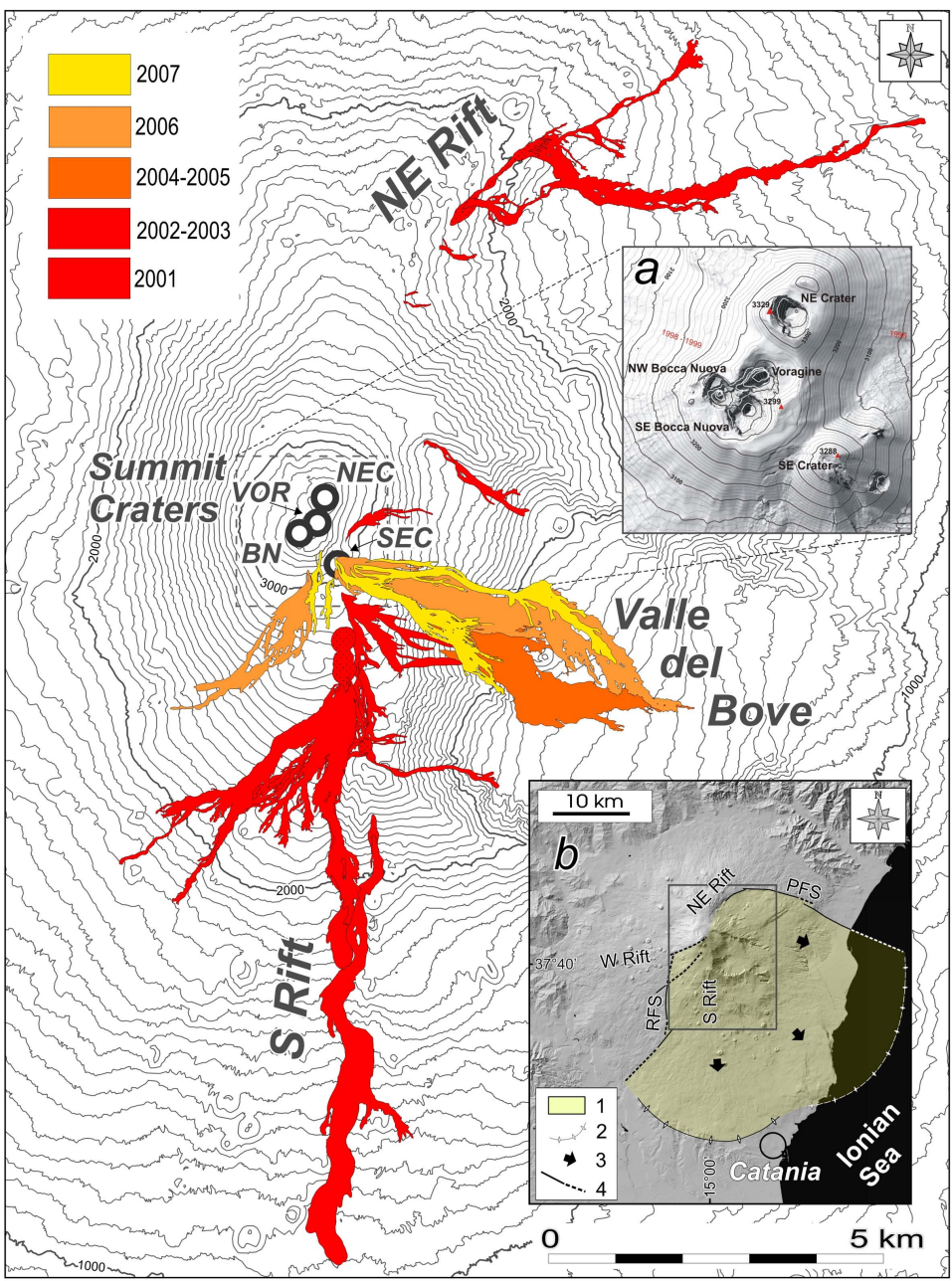


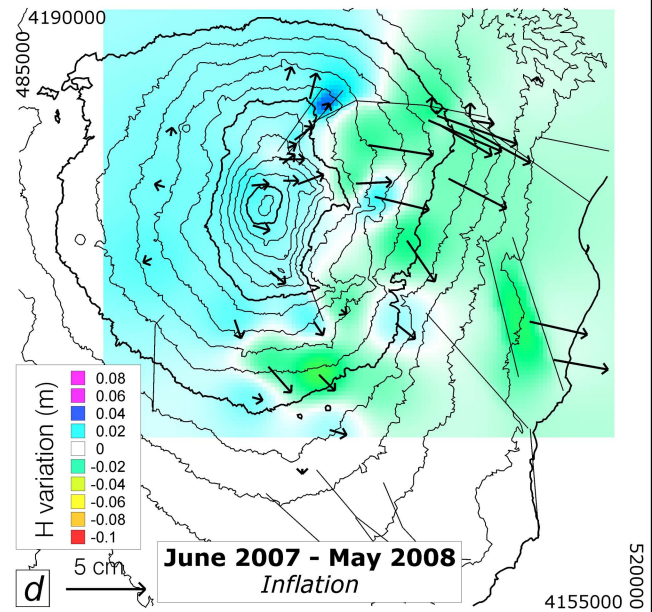
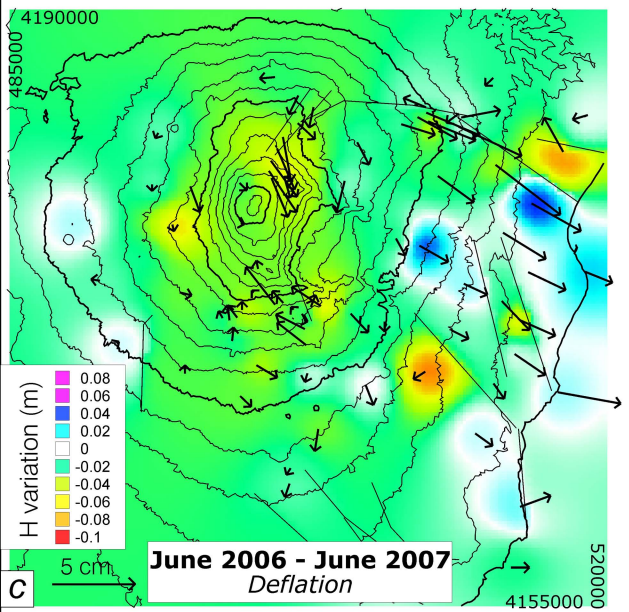
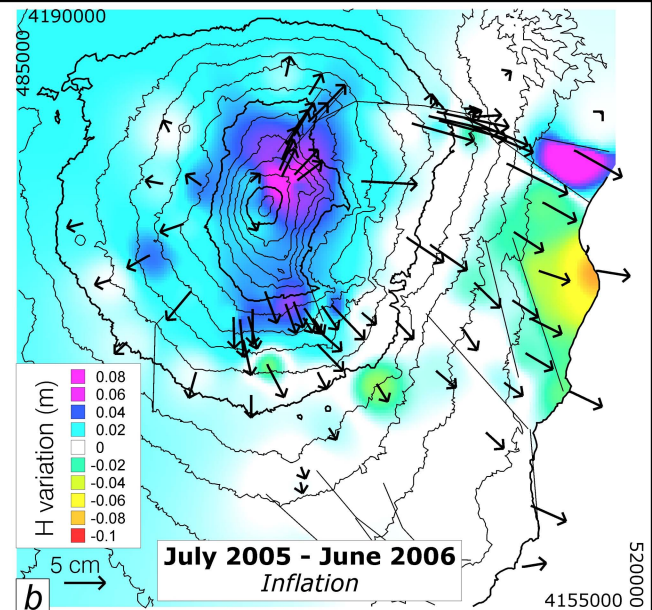
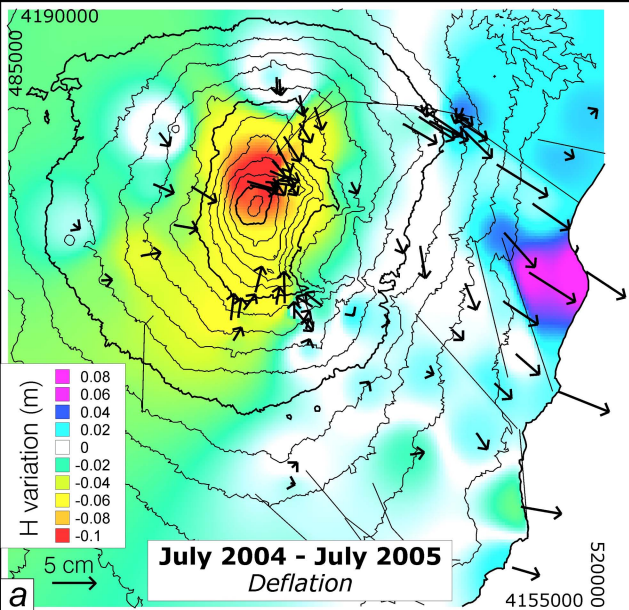
intrusion reached the surface along the western wall of the Valle del Bove, lessening the energy available for propagation of the intrusion in the northern sector. Not in scale.

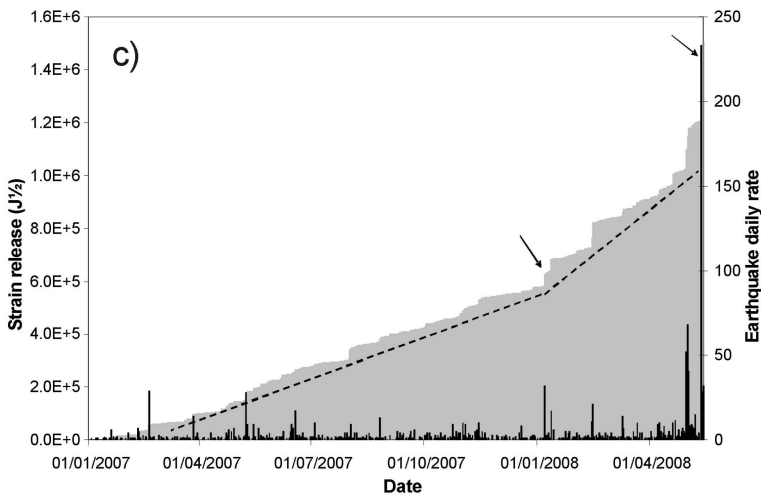
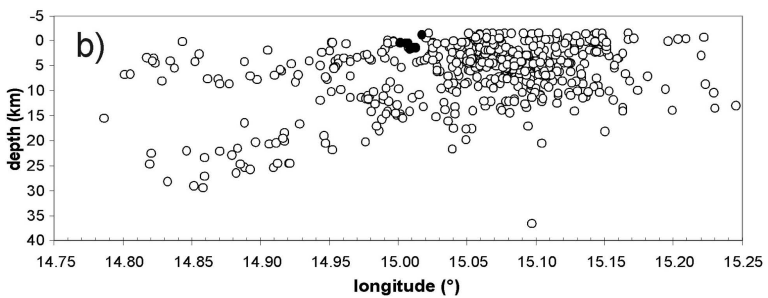
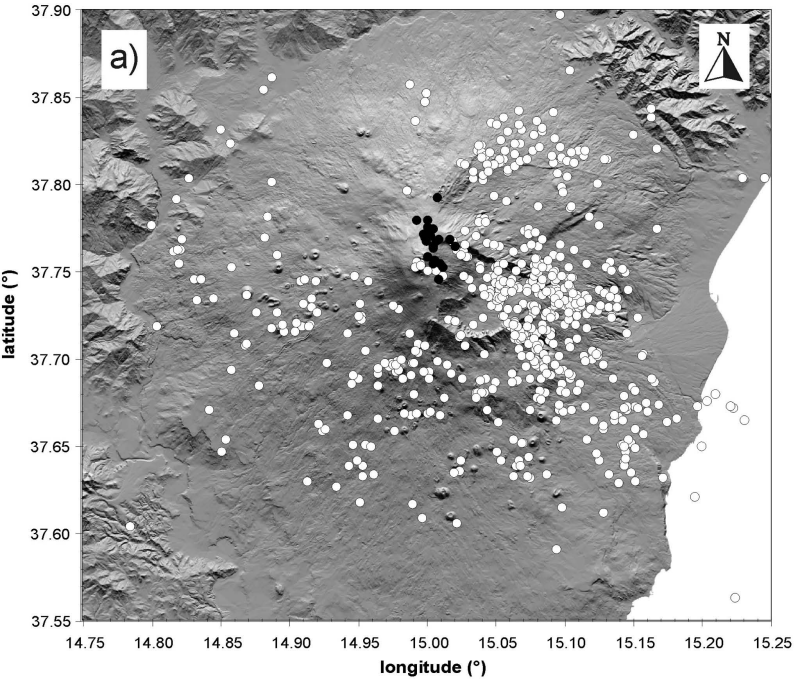
**Table 1** - Physical parameters used in MAGFLOW simulator.

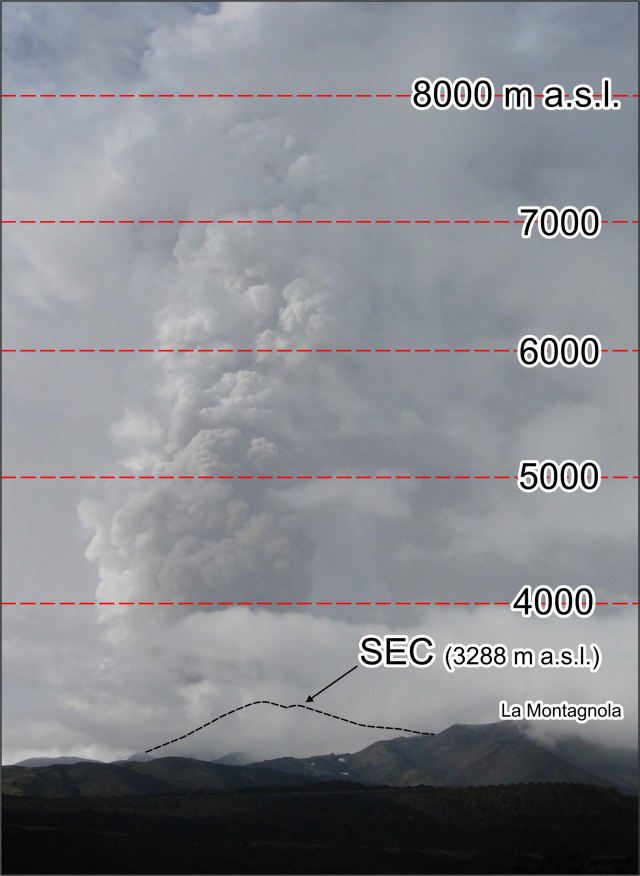
<i>Parameter</i>	<i>Value</i>	<i>Unit</i>
Density ( $\rho$ )	2600	Kg m <sup>-3</sup>
Specific heat capacity (Cp)	1150	J kg <sup>-1</sup> K <sup>-1</sup>
Emissivity ( $\epsilon$ )	0.9	
Solidification Temperature (Ts)	1173	K
Extrusion Temperature (Te)	1360	K

**Table 1** - Physical parameters used in MAGFLOW simulator









8000 m a.s.l.

7000

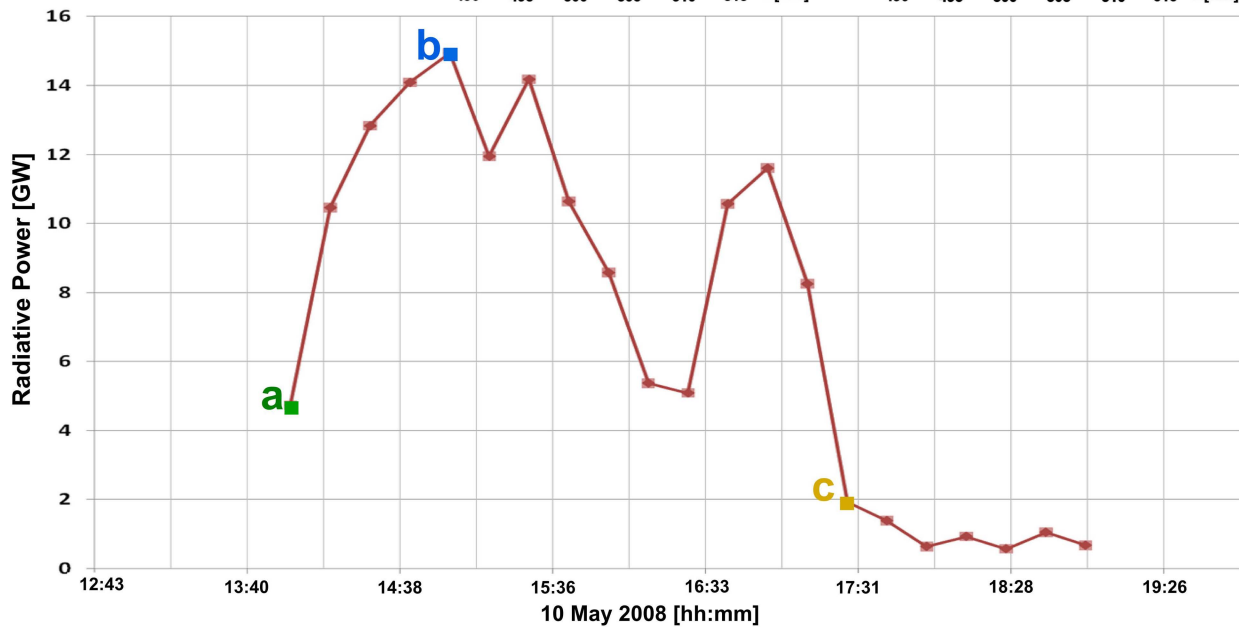
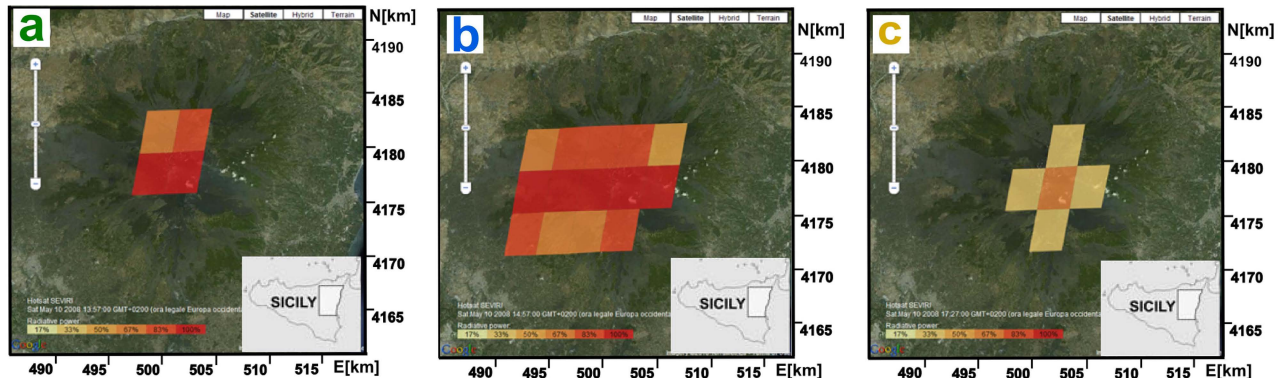
6000

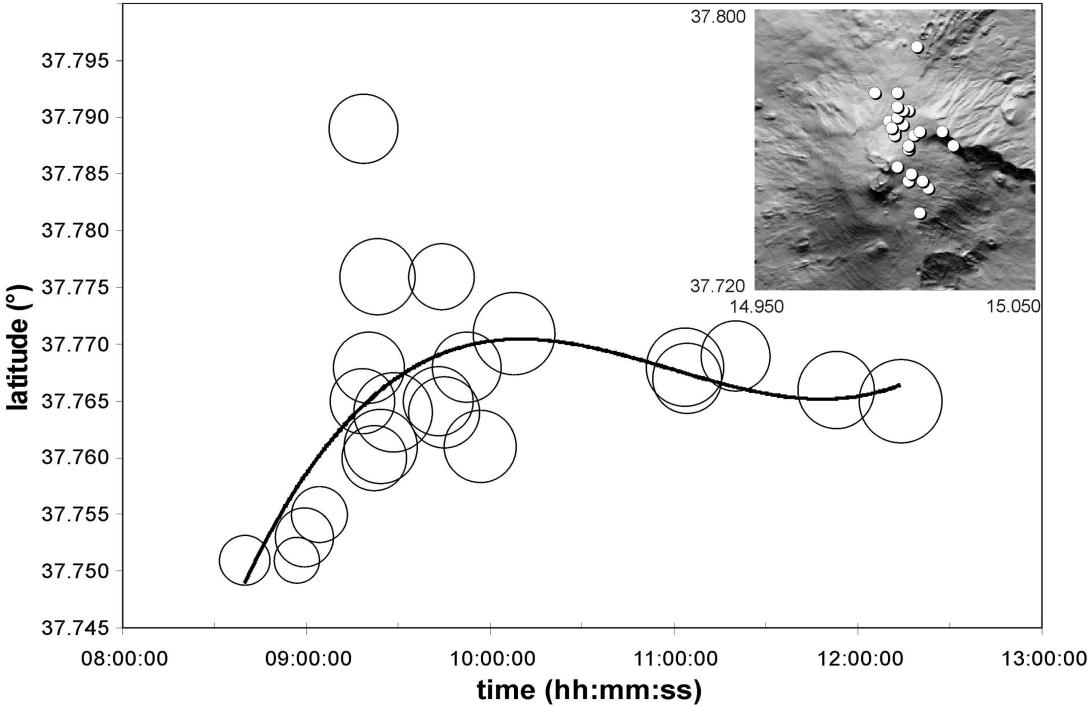
5000

4000

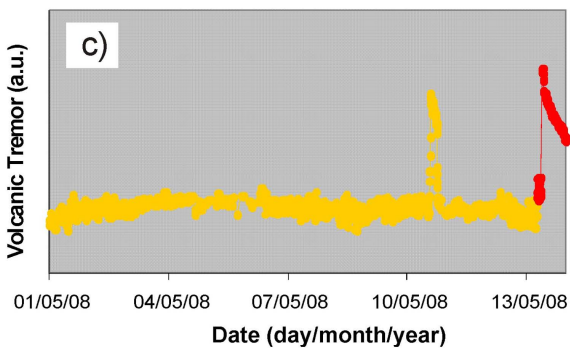
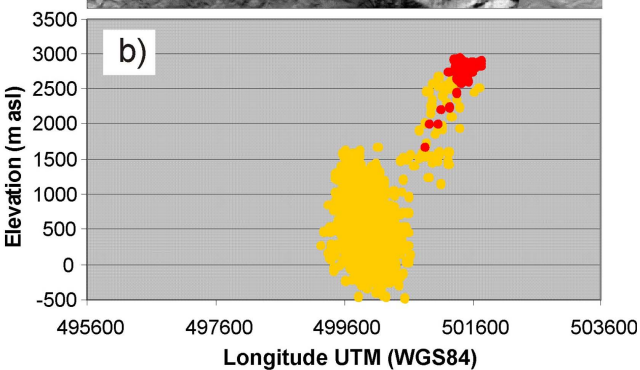
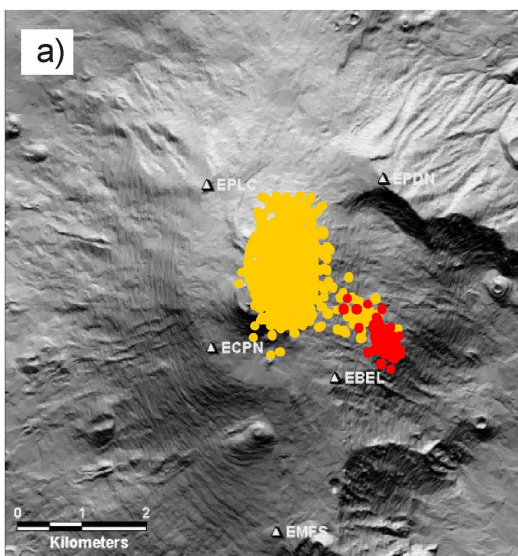
SEC (3288 m a.s.l.)

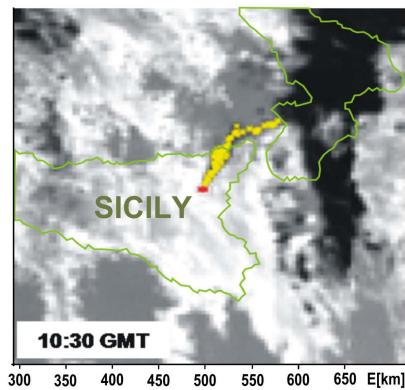
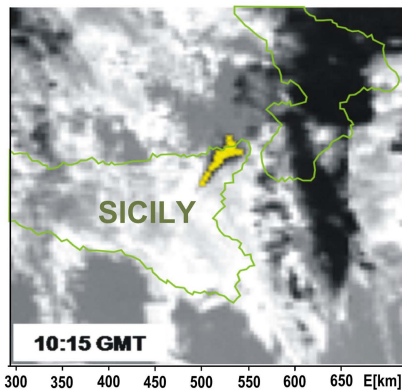
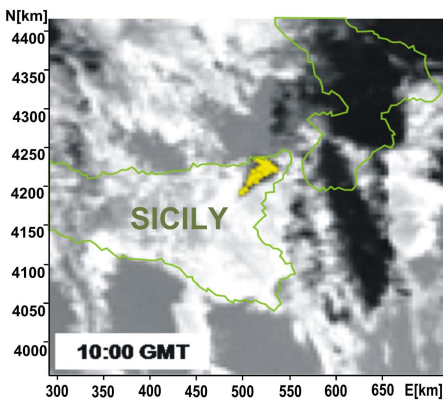
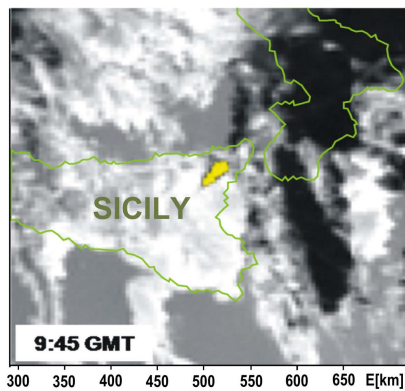
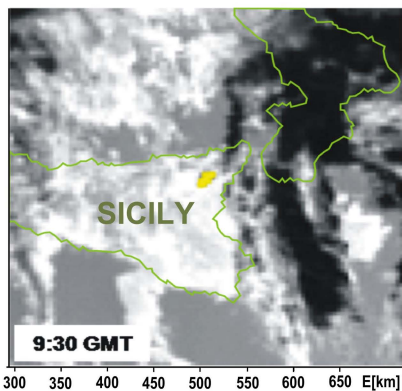
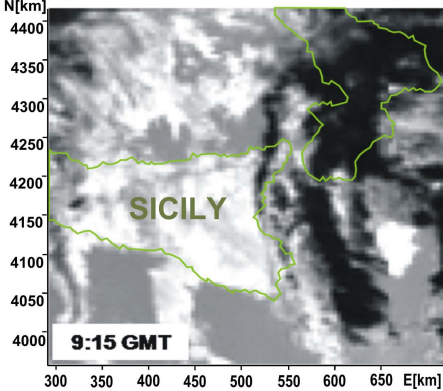
La Montagnola

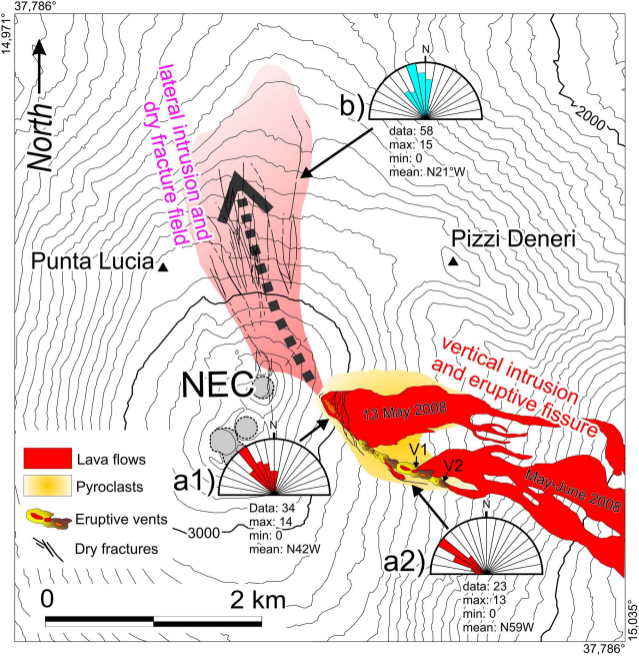


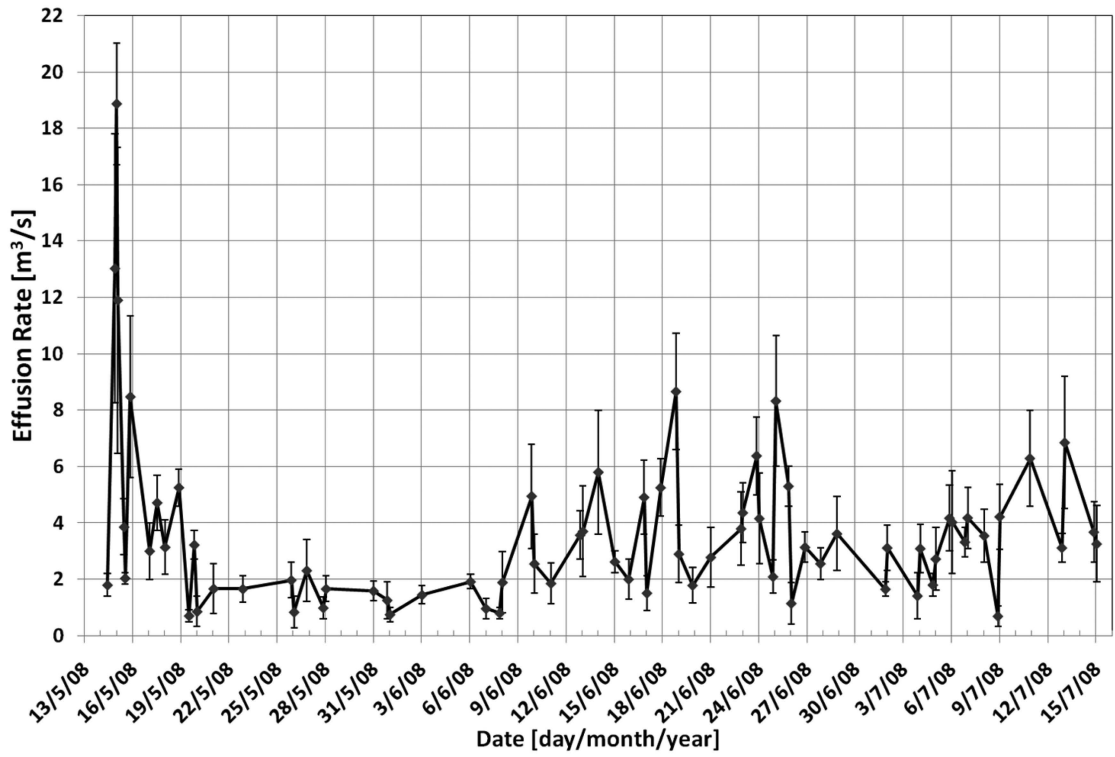


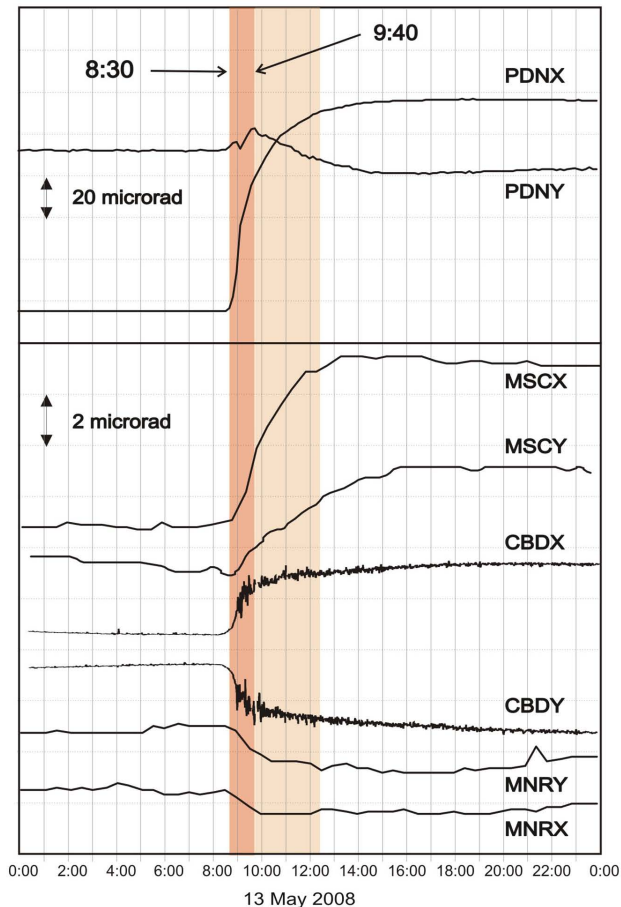
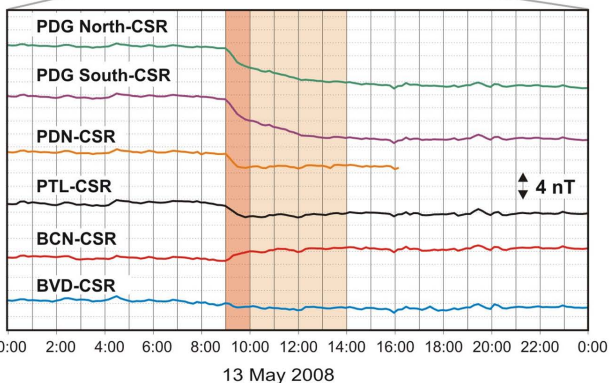
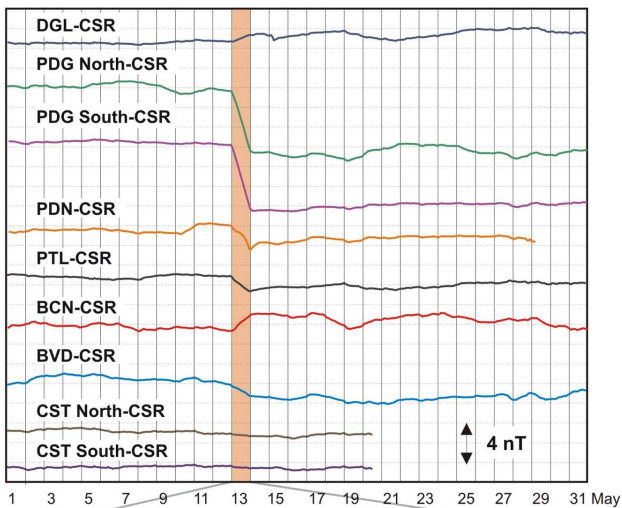


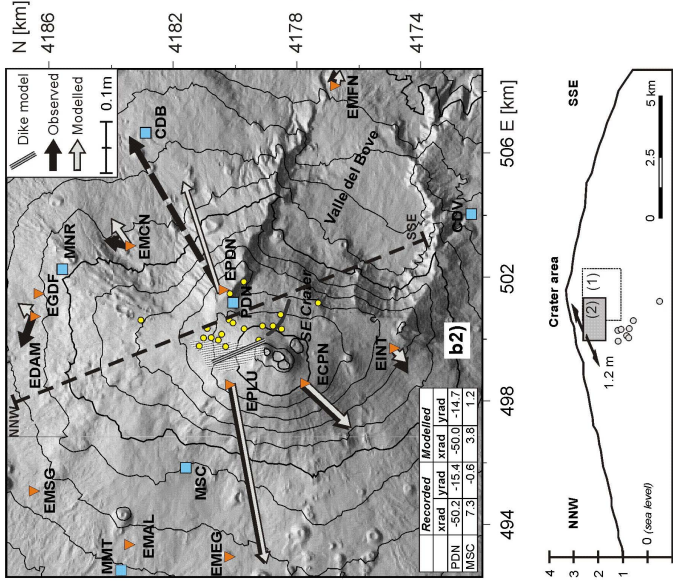
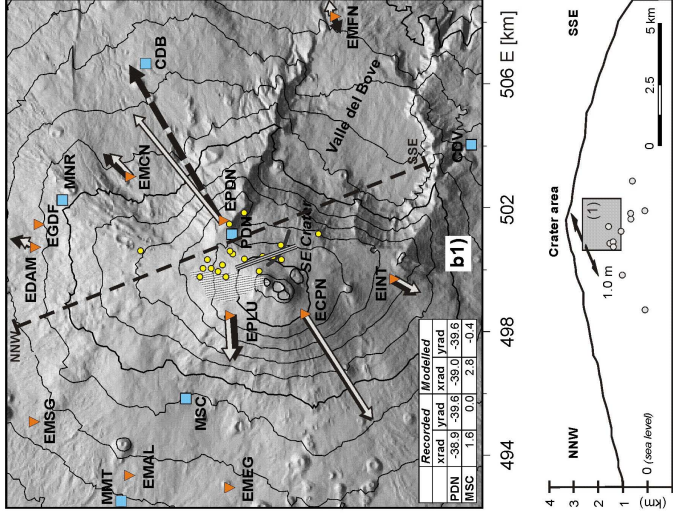
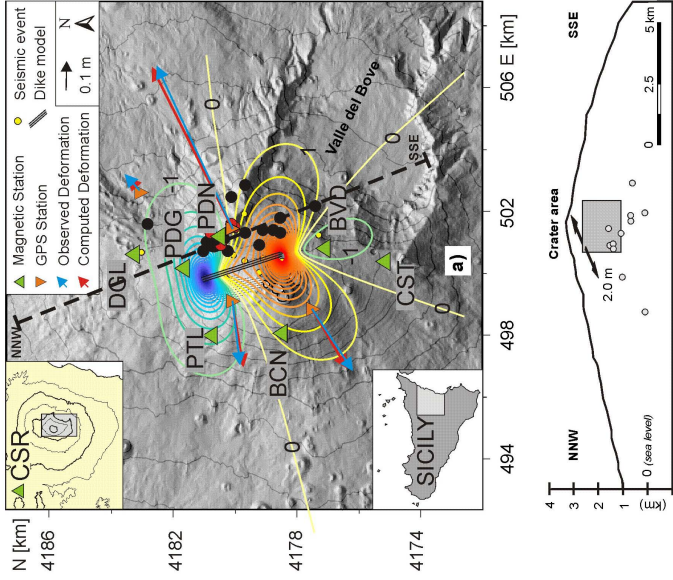


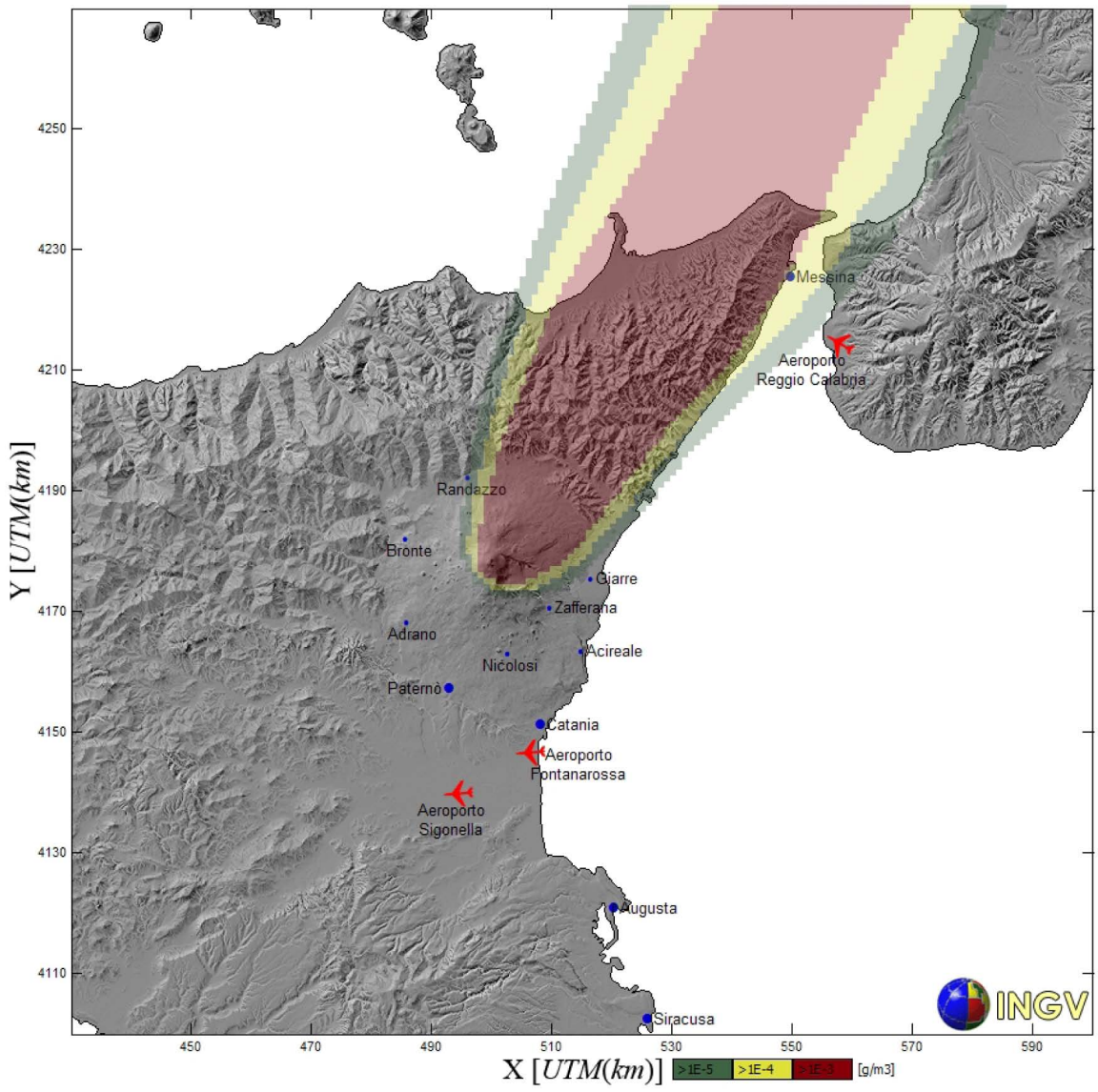












NEC


SEC

V1

V2

Mt  
Centenari

Valle del Bove

 Simulated lava  
flow path

 Observed lava  
flow field

Lava Thickness



High

Medium

Low

